

# 12

## *Ferromagnetism and Antiferromagnetism*

---

<b>FERROMAGNETIC ORDER</b>	<b>323</b>
Curie point and the exchange integral	323
Temperature dependence of the saturation magnetization	326
Saturation magnetization at absolute zero	328
<b>MAGNONS</b>	<b>330</b>
Quantization of spin waves	333
Thermal excitation of magnons	334
<b>NEUTRON MAGNETIC SCATTERING</b>	<b>335</b>
<b>FERRIMAGNETIC ORDER</b>	<b>336</b>
Curie temperature and susceptibility of ferrimagnets	338
Iron garnets	339
<b>ANTIFERROMAGNETIC ORDER</b>	<b>340</b>
Susceptibility below the Néel temperature	343
Antiferromagnetic magnons	344
<b>FERROMAGNETIC DOMAINS</b>	<b>346</b>
Anisotropy energy	348
Transition region between domains	349
Origin of domains	351
Coercivity and hysteresis	352
<b>SINGLE-DOMAIN PARTICLES</b>	<b>354</b>
Geomagnetism and biomagnetism	355
Magnetic force microscopy	355

**NOTATION:** (CGS)  $B = H + 4\pi M$ ; (SI)  $B = \mu_0(H + M)$ . We call  $B_a$  the applied magnetic field in both systems of units: in CGS we have  $B_a = H_a$  and in SI we have  $B_a = \mu_0 H_a$ . The susceptibility is  $\chi = M/B_a$  in CGS and  $\chi = M/H_a = \mu_0 M/B_a$  in SI. One tesla =  $10^4$  gauss.

**SUMMARY**

**356**

**PROBLEMS**

**357**

1. Magnon dispersion relation	357
2. Heat capacity of magnons	357
3. Néel temperature	357
4. Magnetoelastic coupling	357
5. Coercive force of a small particle	358
6. Saturation magnetization near $T_c$	358
7. Néel wall	358
8. Giant magnetoresistance	359

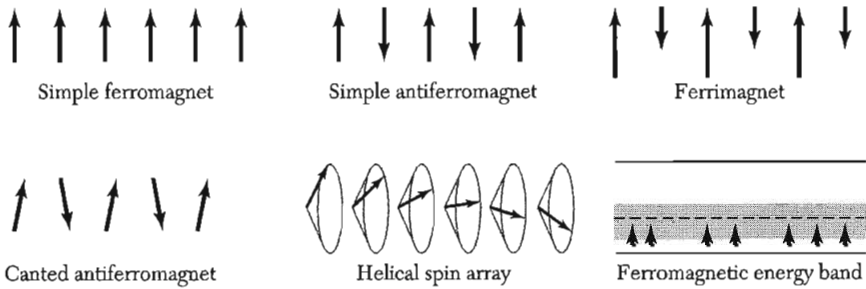


**Figure 1** Ordered arrangements of electron spins.

### FERROMAGNETIC ORDER

A ferromagnet has a spontaneous magnetic moment—a magnetic moment even in zero applied magnetic field. The existence of a spontaneous moment suggests that electron spins and magnetic moments are arranged in a regular manner. The order need not be simple: all of the spin arrangements sketched in Fig. 1 except the simple antiferromagnet have a spontaneous magnetic moment, called the **saturation moment**.

#### *Curie Point and the Exchange Integral*

Consider a paramagnet with a concentration of  $N$  ions of spin  $S$ . Given an internal interaction tending to line up the magnetic moments parallel to each other, we shall have a ferromagnet. Let us postulate such an interaction and call it the **exchange field**.<sup>1</sup> The orienting effect of the exchange field is opposed by thermal agitation, and at elevated temperatures the spin order is destroyed.

We treat the exchange field as equivalent to a magnetic field  $\mathbf{B}_E$ . The magnitude of the exchange field may be as high as  $10^7$  gauss ( $10^3$  tesla). We assume that  $\mathbf{B}_E$  is proportional to the magnetization  $\mathbf{M}$ .

The magnetization is defined as the magnetic moment per unit volume; unless otherwise specified it is understood to be the value in thermal equilibrium at the temperature  $T$ . If domains (regions magnetized in different directions) are present, the magnetization refers to the value within a domain.

In the **mean-field approximation** we assume each magnetic atom experiences a field proportional to the magnetization:

$$\mathbf{B}_E = \lambda \mathbf{M} \quad , \quad (1)$$

where  $\lambda$  is a constant, independent of temperature. According to (1), each spin sees the average magnetization of all the other spins. In truth, it may see only near neighbors, but our simplification is good for a first look at the problem.

The **Curie temperature**  $T_c$  is the temperature above which the spontaneous magnetization vanishes; it separates the disordered paramagnetic phase at  $T > T_c$  from the ordered ferromagnetic phase at  $T < T_c$ . We can find  $T_c$  in terms of the constant  $\lambda$  in (1).

<sup>1</sup>Also called the molecular field or the Weiss field, after Pierre Weiss who was the first to imagine such a field. The exchange field  $\mathbf{B}_E$  simulates a real magnetic field in the expressions for the energy  $-\boldsymbol{\mu} \cdot \mathbf{B}_E$  and the torque  $\boldsymbol{\mu} \times \mathbf{B}_E$  on a magnetic moment  $\boldsymbol{\mu}$ . But  $\mathbf{B}_E$  is not really a magnetic field and therefore does not enter into the Maxwell equations; for example, there is no current density  $\mathbf{j}$  related to  $\mathbf{B}_E$  by  $\text{curl } \mathbf{H} = 4\pi\mathbf{j}/c$ . The magnitude of  $\mathbf{B}_E$  is typically  $10^4$  larger than the average magnetic field of the magnetic dipoles of the ferromagnet.

Consider the paramagnetic phase: an applied field  $B_a$  will cause a finite magnetization and this in turn will cause a finite exchange field  $B_E$ . If  $\chi_p$  is the paramagnetic susceptibility,

$$\text{(CGS)} \quad M = \chi_p(B_a + B_E) ; \quad \text{(SI)} \quad \mu_0 M = \chi_p(B_a + B_E) . \quad (2)$$

The magnetization is equal to a constant susceptibility times a field only if the fractional alignment is small: this is where the assumption enters that the specimen is in the paramagnetic phase.

The paramagnetic susceptibility (Chapt. 11) is given by the Curie law  $\chi_p = C/T$ , where  $C$  is the Curie constant. Substitute (1) in (2); we find  $MT = C(B_a + \lambda M)$  and

$$\text{(CGS)} \quad \chi = \frac{M}{B_a} = \frac{C}{(T - C\lambda)} . \quad (3)$$

The susceptibility (3) has a singularity at  $T = C\lambda$ . At this temperature (and below) there exists a spontaneous magnetization, because if  $\chi$  is infinite we can have a finite  $M$  for zero  $B_a$ . From (3) we have the **Curie-Weiss law**

$$\text{(CGS)} \quad \chi = \frac{C}{T - T_c} ; \quad T_c = C\lambda . \quad (4)$$

This expression describes fairly well the observed susceptibility variation in the paramagnetic region above the Curie point. The reciprocal susceptibility of nickel is plotted in Fig. 2.

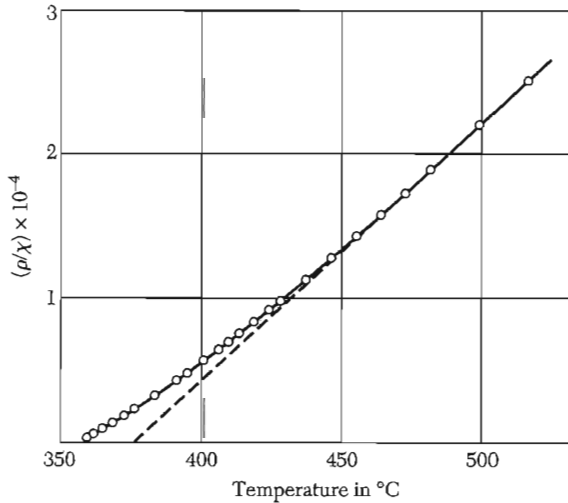


**Figure 2** Reciprocal of the susceptibility per gram of nickel in the neighborhood of the Curie temperature (358°C). The density is  $\rho$ . The dashed line is a linear extrapolation from high temperatures. (After P. Weiss and R. Forrer.)

From (4) and the definition (11.22) of the Curie constant  $C$  we may determine the value of the mean field constant  $\lambda$  in (1):

$$\text{(CGS)} \quad \lambda = \frac{T_c}{C} = \frac{3k_B T_c}{Ng^2 S(S+1)\mu_B^2}. \quad (5)$$

For iron  $T_c \approx 1000$  K,  $g \approx 2$ , and  $S \approx 1$ ; from (5) we have  $\lambda \approx 5000$ . With  $M_s \approx 1700$  we have  $B_R \approx \lambda M \approx (5000)(1700) \approx 10^7$  G =  $10^3$  T. The exchange field in iron is very much stronger than the real magnetic field due to the other magnetic ions in the crystal: a magnetic ion produces a field  $\approx \mu_B/a^3$  or about  $10^3$  G = 0.1 T at a neighboring lattice point.

The exchange field gives an approximate representation of the quantum-mechanical exchange interaction. On certain assumptions it is shown in texts on quantum theory that the energy of interaction of atoms  $i, j$  bearing electron spins  $S_i, S_j$  contains a term

$$U = -2JS_i \cdot S_j, \quad (6)$$

where  $J$  is the exchange integral and is related to the overlap of the charge distributions of the atoms  $i, j$ . Equation (6) is called the **Heisenberg model**.

The charge distribution of a system of two spins depends on whether the spins are parallel or antiparallel<sup>2</sup> for the Pauli principle excludes two electrons of the same spin from being at the same place at the same time. It does not exclude two electrons of opposite spin. Thus the electrostatic energy of a system will depend on the relative orientation of the spins: the difference in energy defines the **exchange energy**.

The exchange energy of two electrons may be written in the form  $-2J\mathbf{s}_1 \cdot \mathbf{s}_2$  as in (6), just as if there were a direct coupling between the directions of the two spins. For many purposes in ferromagnetism it is a good approximation to treat the spins as classical angular momentum vectors.

We can establish an approximate connection between the exchange integral  $J$  and the Curie temperature  $T_c$ . Suppose that the atom under consideration has  $z$  nearest neighbors, each connected with the central atom by the interaction  $J$ . For more distant neighbors we take  $J$  as zero. The mean field theory result is

$$J = \frac{3k_B T_c}{2zS(S+1)}. \quad (7)$$

Better statistical approximations give somewhat different results. For the sc, bcc, and fcc structures with  $S = \frac{1}{2}$ , Rushbrooke and Wood give

<sup>2</sup>If two spins are antiparallel, the wavefunctions of the two electrons must be symmetric, as in the combination  $u(\mathbf{r}_1)v(\mathbf{r}_2) + u(\mathbf{r}_2)v(\mathbf{r}_1)$ . If the two spins are parallel, the Pauli principle requires that the orbital part of the wavefunction be antisymmetric, as in  $u(\mathbf{r}_1)v(\mathbf{r}_2) - u(\mathbf{r}_2)v(\mathbf{r}_1)$ , for here if we interchange the coordinates  $\mathbf{r}_1, \mathbf{r}_2$  the wavefunction changes sign. If we set the positions equal so that  $\mathbf{r}_1 = \mathbf{r}_2$  then the antisymmetric function vanishes: for parallel spins there is zero probability of finding the two electrons at the same position.

$k_B T_c / zJ = 0.28$ ;  $0.325$ ; and  $0.346$ , respectively, as compared with  $0.500$  from (7) for all three structures. If iron is represented by the Heisenberg model with  $S = 1$ , then the observed Curie temperature corresponds to  $J = 11.9$  meV.

### Temperature Dependence of the Saturation Magnetization

We can also use the mean field approximation below the Curie temperature to find the magnetization as a function of temperature. We proceed as before, but instead of the Curie law we use the complete Brillouin expression for the magnetization. For spin  $\frac{1}{2}$  this is  $M = N\mu \tanh(\mu B/k_B T)$ .

If we omit the applied magnetic field and replace  $B$  by the molecular field  $B_E = \lambda M$ , then

$$M = N\mu \tanh(\mu\lambda M/k_B T) . \quad (8)$$

We shall see that solutions of this equation with nonzero  $M$  exist in the temperature range between  $0$  and  $T_c$ .

To solve (8) we write it in terms of the reduced magnetization  $m \equiv M/N\mu$  and the reduced temperature  $t = k_B T/N\mu^2\lambda$ , whence

$$m = \tanh(m/t) . \quad (9)$$

We then plot the right and left sides of this equation separately as functions of  $m$ , as in Fig. 3. The intercept of the two curves gives the value of  $m$  at the temperature of interest. The critical temperature is  $t = 1$ , or  $T_c = N\mu^2\lambda/k_B$ .

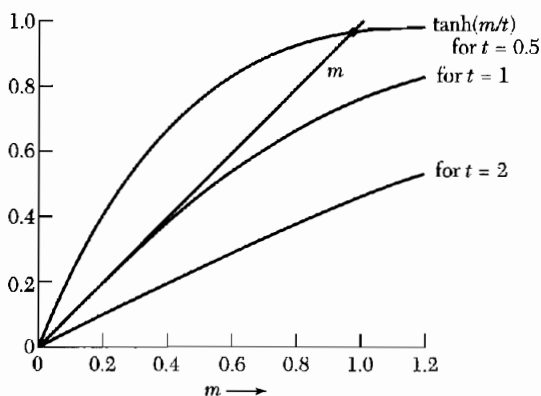


**Figure 3** Graphical solution of Eq. (9) for the reduced magnetization  $m$  as a function of temperature. The reduced magnetization is defined as  $m = M/N\mu$ . The left-hand side of Eq. (9) is plotted as a straight line  $m$  with unit slope. The right-hand side is  $\tanh(m/t)$  and is plotted vs.  $m$  for three different values of the reduced temperature  $t = k_B T/N\mu^2\lambda = T/T_c$ . The three curves correspond to the temperatures  $2T_c$ ,  $T_c$ , and  $0.5T_c$ . The curve for  $t = 2$  intersects the straight line  $m$  only at  $m = 0$ , as appropriate for the paramagnetic region (there is no external applied magnetic field). The curve for  $t = 1$  (or  $T = T_c$ ) is tangent to the straight line  $m$  at the origin; this temperature marks the onset of ferromagnetism. The curve for  $t = 0.5$  is in the ferromagnetic region and intersects the straight line  $m$  at about  $m = 0.94N\mu$ . As  $t \rightarrow 0$  the intercept moves up to  $m = 1$ , so that all magnetic moments are lined up at absolute zero.

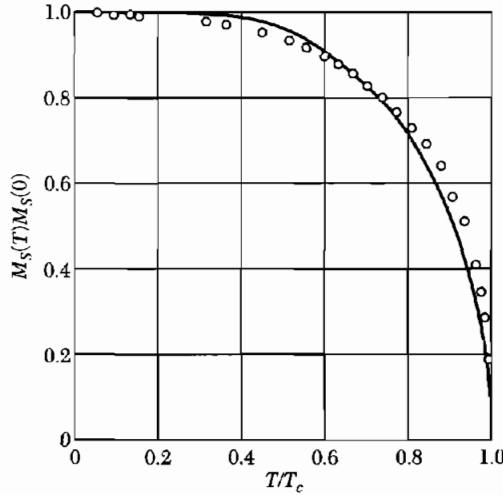


**Figure 4** Saturation magnetization of nickel as a function of temperature, together with the theoretical curve for  $S = \frac{1}{2}$  on the mean field theory. Experimental values by P. Weiss and R. Forrer.

The curves of  $M$  versus  $T$  obtained in this way reproduce roughly the features of the experimental results, as shown in Fig. 4 for nickel. As  $T$  increases, the magnetization decreases smoothly to zero at  $T = T_c$ . This behavior classifies the usual ferromagnetic/paramagnetic transition as a second-order transition.

The mean-field theory does not give a good description of the variation of  $M$  at low temperatures. For  $T \ll T_c$  the argument of  $\tanh$  in (9) is large, and

$$\tanh \xi \cong 1 - 2e^{-2\xi} \dots$$

To lowest order the magnetization deviation  $\Delta M = M(0) - M(T)$  is

$$\Delta M \cong 2N\mu \exp(-2\lambda N\mu^2/k_B T) . \quad (10)$$

The argument of the exponential is equal to  $-2T_c/T$ . For  $T = 0.1T_c$  we have  $\Delta M/N\mu \cong 4 \times 10^{-9}$ .

The experimental results show a much more rapid dependence of  $\Delta M$  on temperature at low temperatures. At  $T = 0.1T_c$  we have  $\Delta M/M \cong 2 \times 10^{-3}$  from the data of Fig. 5. The leading term in  $\Delta M$  is observed from experiment to have the form

$$\Delta M/M(0) = AT^{3/2} , \quad (11)$$

where the constant  $A$  has the experimental value  $(7.5 \pm 0.2) \times 10^{-6} \text{ deg}^{-3/2}$  for Ni and  $(3.4 \pm 0.2) \times 10^{-6} \text{ deg}^{-3/2}$  for Fe. The result (11) finds a natural explanation in terms of spin wave theory.

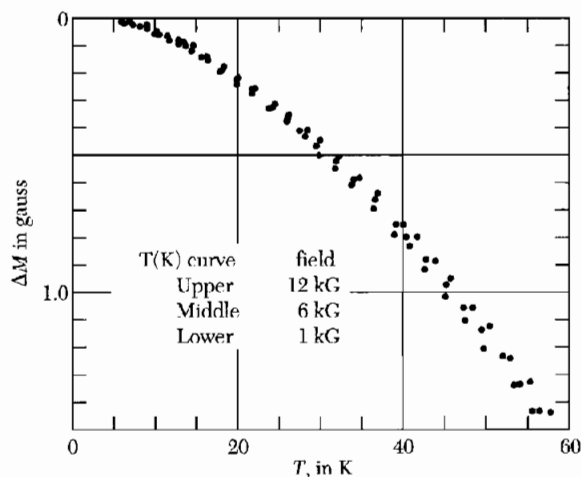


**Figure 5** Decrease in magnetization of nickel with temperature, after Argyle, Charap, and Pugh. In the plot  $\Delta M = 0$  at 4.2 K.

### Saturation Magnetization at Absolute Zero

Table 1 gives representative values of the saturation magnetization  $M_s$ , the ferromagnetic Curie temperature, and the effective magneton number defined by  $M_s(0) = n_B N \mu_B$ , where  $N$  is the number of formula units per unit volume. Do not confuse  $n_B$  with the paramagnetic effective magneton number  $p$  defined by (11.23).

**Table 1** Ferromagnetic crystals

Substance	Magnetization $M_s$ , in gauss		$n_B(0\text{ K})$ , per formula unit	Curie temperature, in K
	Room temperature	0 K		
Fe	1707	1740	2.22	1043
Co	1400	1446	1.72	1388
Ni	485	510	0.606	627
Gd	—	2060	7.63	292
Dy	—	2920	10.2	88
MnAs	670	870	3.4	318
MnBi	620	680	3.52	630
MnSb	710	—	3.5	587
CrO <sub>2</sub>	515	—	2.03	386
MnOF <sub>2</sub> O <sub>3</sub>	410	—	5.0	573
FeOF <sub>2</sub> O <sub>3</sub>	480	—	4.1	858
NiOF <sub>2</sub> O <sub>3</sub>	270	—	2.4	(858)
CuOF <sub>2</sub> O <sub>3</sub>	135	—	1.3	728
MgOF <sub>2</sub> O <sub>3</sub>	110	—	1.1	713
EuO	—	1920	6.8	69
Y <sub>3</sub> Fe <sub>5</sub> O <sub>12</sub>	130	200	5.0	560

Observed values of  $n_B$  are often nonintegral. There are several possible causes. One is the spin-orbit interaction which adds or subtracts some orbital magnetic moment. Another cause in ferromagnetic metals is the conduction electron magnetization induced locally about a paramagnetic ion core. A third cause is suggested by the drawing in Fig. 1 of the spin arrangement in a ferrimagnet: if there is one atom of spin projection  $-S$  for every two atoms  $+S$ , the average spin is  $\frac{1}{3}S$ .

Are there in fact any simple ferromagnetic insulators, with all ionic spins parallel in the ground state? The few simple ferromagnets known at present include  $\text{CrBr}_3$ ,  $\text{EuO}$ , and  $\text{EuS}$ .

A band or itinerant electron model accounts for the ferromagnetism of the transition metals Fe, Co, Ni. The approach is indicated in Figs. 6 and 7. The relationship of  $4s$  and  $3d$  bands is shown in Fig. 6 for copper, which is not ferromagnetic. If we remove one electron from copper, we obtain nickel which has the possibility of a hole in the  $3d$  band. In the band structure of nickel shown in Fig. 7a for  $T > T_c$  we have taken  $2 \times 0.27 = 0.54$  of an electron away from the  $3d$  band and  $0.46$  away from the  $4s$  band, as compared with copper.

The band structure of nickel at absolute zero is shown in Fig. 7b. Nickel is ferromagnetic, and at absolute zero  $n_B = 0.60$  Bohr magnetons per atom. After allowance for the magnetic moment contribution of orbital electronic motion, nickel has an excess of  $0.54$  electron per atom having spin preferentially oriented in one direction. The exchange enhancement of the susceptibility of metals was the subject of Problem 11.6.

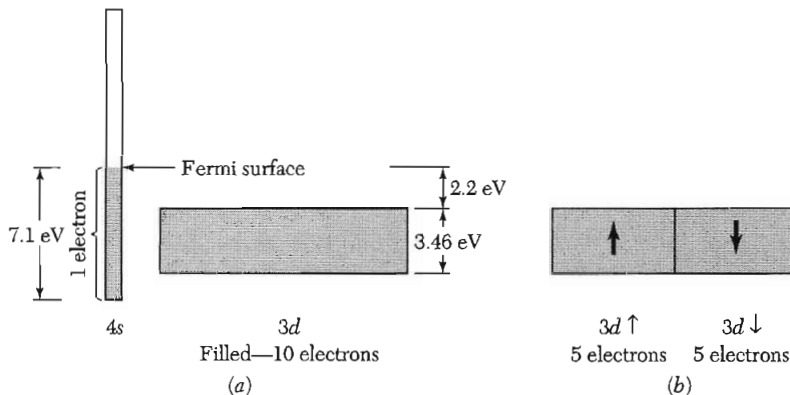


**Figure 6a** Schematic relationship of  $4s$  and  $3d$  bands in metallic copper. The  $3d$  band holds 10 electrons per atom and is filled. The  $4s$  band can hold two electrons per atom; it is shown half-filled, as copper has one valence electron outside the filled  $3d$  shell.

**Figure 6b** The filled  $3d$  band of copper shown as two separate sub-bands of opposite electron spin orientation, each band holding five electrons. With both sub-bands filled as shown, the net spin (and hence the net magnetization) of the  $d$  band is zero.

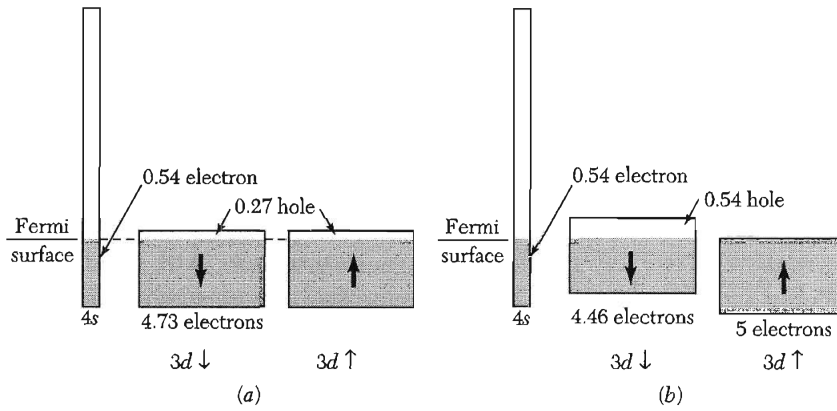


**Figure 7a** Band relationships in nickel above the Curie temperature. The net magnetic moment is zero, as there are equal numbers of holes in the  $3d \downarrow$  and  $3d \uparrow$  bands.

**Figure 7b** Schematic relationship of bands in nickel at absolute zero. The energies of the  $3d \uparrow$  and  $3d \downarrow$  sub-bands are separated by an exchange interaction. The  $3d \uparrow$  band is filled; the  $3d \downarrow$  band contains 4.46 electrons and 0.54 hole. The  $4s$  band is usually thought to contain approximately equal numbers of electrons in both spin directions, and so we have not troubled to divide it into sub-bands. The net magnetic moment of  $0.54 \mu_B$  per atom arises from the excess population of the  $3d \uparrow$  band over the  $3d \downarrow$  band. It is often convenient to speak of the magnetization as arising from the 0.54 hole in the  $3d \downarrow$  band.

## MAGNONS

A magnon is a quantized spin wave. We use a classical argument, just as we did for phonons, to find the magnon dispersion relation for  $\omega$  versus  $k$ . We then quantize the magnon energy and interpret the quantization in terms of spin reversal.

The ground state of a simple ferromagnet has all spins parallel, as in Fig. 8a. Consider  $N$  spins each of magnitude  $S$  on a line or a ring, with nearest-neighbor spins coupled by the Heisenberg interaction:

$$U = -2J \sum_{p=1}^N \mathbf{S}_p \cdot \mathbf{S}_{p+1} . \quad (12)$$

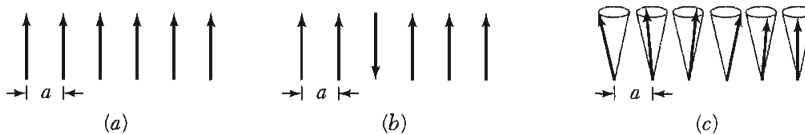


**Figure 8** (a) Classical picture of the ground state of a simple ferromagnet; all spins are parallel. (b) A possible excitation; one spin is reversed. (c) The low-lying elementary excitations are spin waves. The ends of the spin vectors precess on the surfaces of cones, with successive spins advanced in phase by a constant angle.

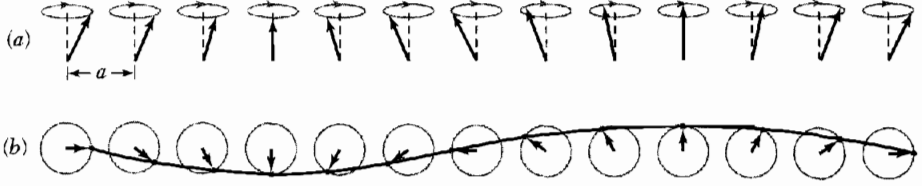


**Figure 9** A spin wave on a line of spins. (a) The spins viewed in perspective. (b) Spins viewed from above, showing one wavelength. The wave is drawn through the ends of the spin vectors.

Here  $J$  is the exchange integral and  $\hbar\mathbf{S}_p$  is the angular momentum of the spin at site  $p$ . If we treat the spins  $\mathbf{S}_p$  as classical vectors, then in the ground state  $\mathbf{S}_p \cdot \mathbf{S}_{p+1} = S^2$  and the exchange energy of the system is  $U_0 = -2NJS^2$ .

What is the energy of the first excited state? Consider an excited state with one particular spin reversed, as in Fig. 8b. We see from (12) that this increases the energy by  $8JS^2$ , so that  $U_1 = U_0 + 8JS^2$ . But we can form an excitation of much lower energy if we let all the spins share the reversal, as in Fig. 8c. The elementary excitations of a spin system have a wavelike form and are called magnons (Fig. 9). These are analogous to lattice vibrations or phonons. Spin waves are oscillations in the relative orientations of spins on a lattice; lattice vibrations are oscillations in the relative positions of atoms on a lattice.

We now give a classical derivation of the magnon dispersion relation. The terms in (12) which involve the  $p$ th spin are

$$-2J\mathbf{S}_p \cdot (\mathbf{S}_{p-1} + \mathbf{S}_{p+1}) . \quad (13)$$

We write magnetic moment at site  $p$  as  $\boldsymbol{\mu}_p = -g\mu_B\mathbf{S}_p$ . Then (13) becomes

$$-\boldsymbol{\mu}_p \cdot [(-2J/g\mu_B)(\mathbf{S}_{p-1} + \mathbf{S}_{p+1})] , \quad (14)$$

which is of the form  $-\boldsymbol{\mu}_p \cdot \mathbf{B}_p$ , where the effective magnetic field or exchange field that acts on the  $p$ th spin is

$$\mathbf{B}_p = (-2J/g\mu_B)(\mathbf{S}_{p-1} + \mathbf{S}_{p+1}) . \quad (15)$$

From mechanics the rate of change of the angular momentum  $\hbar\mathbf{S}_p$  is equal to the torque  $\boldsymbol{\mu}_p \times \mathbf{B}_p$  which acts on the spin:  $\hbar d\mathbf{S}_p/dt = \boldsymbol{\mu}_p \times \mathbf{B}_p$ , or

$$d\mathbf{S}_p/dt = (-g\mu_B/\hbar)\mathbf{S}_p \times \mathbf{B}_p = (2J/\hbar)(\mathbf{S}_p \times \mathbf{S}_{p-1} + \mathbf{S}_p \times \mathbf{S}_{p+1}) . \quad (16)$$

In Cartesian components

$$dS_p^x/dt = (2J/\hbar)[S_p^y(S_{p-1}^z + S_{p+1}^z) - S_p^z(S_{p-1}^y + S_{p+1}^y)] , \quad (17)$$

and similarly for  $dS_p^y/dt$  and  $dS_p^z/dt$ . These equations involve products of spin components and are nonlinear.

If the amplitude of the excitation is small (if  $S_p^x, S_p^y \ll S$ ), we may obtain an approximate set of linear equations by taking all  $S_p^z = S$  and by neglecting terms in the product of  $S^x$  and  $S^y$  which appear in the equation for  $dS^z/dt$ . The linearized equations are

$$dS_p^x/dt = (2JS/\hbar)(2S_p^y - S_{p-1}^y - S_{p+1}^y) ; \quad (18a)$$

$$dS_p^y/dt = -(2JS/\hbar)(2S_p^x - S_{p-1}^x - S_{p+1}^x) ; \quad (18b)$$

$$dS_p^z/dt = 0 . \quad (19)$$

By analogy with phonon problems we look for traveling wave solutions of (18) of the form

$$S_p^x = u \exp[i(pka - \omega t)] ; \quad S_p^y = v \exp[i(pka - \omega t)] , \quad (20)$$

where  $u, v$  are constants,  $p$  is an integer, and  $a$  is the lattice constant. On substitution into (18) we have

$$-i\omega u = (2JS/\hbar)(2 - e^{-ika} - e^{ika})v = (4JS/\hbar)(1 - \cos ka)v ;$$

$$-i\omega v = -(2JS/\hbar)(2 - e^{-ika} - e^{ika})u = -(4JS/\hbar)(1 - \cos ka)u .$$

These equations have a solution for  $u$  and  $v$  if the determinant of the coefficients is equal to zero:

$$\begin{vmatrix} i\omega & (4JS/\hbar)(1 - \cos ka) \\ -(4JS/\hbar)(1 - \cos ka) & i\omega \end{vmatrix} = 0 , \quad (21)$$

whence

$$\hbar\omega = 4JS(1 - \cos ka) . \quad (22)$$

This result is plotted in Fig. 10. With this solution we find that  $v = -iu$ , corresponding to circular precession of each spin about the  $z$  axis. We see this on taking real parts of (20), with  $v$  set equal to  $-iu$ . Then

$$S_p^x = u \cos(pka - \omega t) ; \quad S_p^y = u \sin(pka - \omega t) .$$

Equation (22) is the dispersion relation for spin waves in one dimension with nearest-neighbor interactions. Precisely the same result is obtained from the quantum-mechanical solution; see *QTS*, Chapter 4. At long wavelengths  $ka \ll 1$ , so that  $(1 - \cos ka) \cong \frac{1}{2}(ka)^2$  and

$$\hbar\omega \cong (2JSa^2)k^2 . \quad (23)$$

The frequency is proportional to  $k^2$ ; in the same limit the frequency of a phonon is directly proportional to  $k$ .

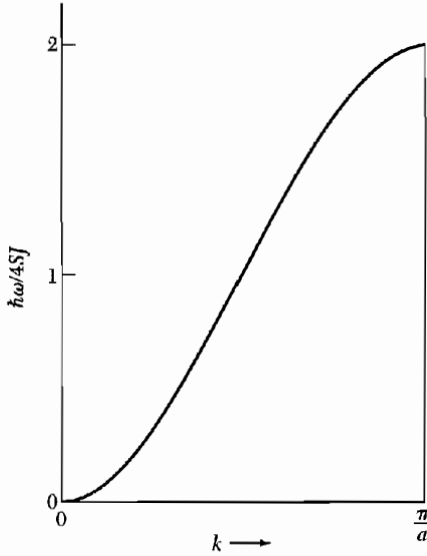


**Figure 10** Dispersion relation for magnons in a ferromagnet in one dimension with nearest-neighbor interactions.

The dispersion relation for a ferromagnetic cubic lattice with nearest-neighbor interactions

$$\hbar\omega = 2JS[z - \sum_{\delta} \cos(\mathbf{k} \cdot \boldsymbol{\delta})] , \quad (24)$$

where the summation is over the  $z$  vectors denoted by  $\boldsymbol{\delta}$  which join the central atom to its nearest neighbors. For  $ka \ll 1$ ,

$$\hbar\omega = (2JSa^2)k^2 \quad (25)$$

for all three cubic lattices, where  $a$  is the lattice constant.

The coefficient of  $k^2$  often may be determined accurately by neutron scattering or by spin wave resonance in thin films, Chapter 13. By neutron scattering G. Shirane and coworkers find, in the equation  $\hbar\omega = Dk^2$ , the values 281, 500, and 364 meV  $\text{\AA}^2$  for  $D$  at 295 K in Fe, Co, and Ni, respectively.

**Quantization of Spin Waves.** The quantization of spin waves proceeds as for photons and phonons. The energy of a mode of frequency  $\omega_k$  with  $n_k$  magnons is given by

$$\epsilon_k = (n_k + \frac{1}{2})\hbar\omega_k . \quad (26)$$

The excitation of a magnon corresponds to the reversal of one spin  $\frac{1}{2}$ .

### Thermal Excitation of Magnons

In thermal equilibrium the average value of the number of magnons excited in the mode  $\mathbf{k}$  is given by the Planck distribution<sup>3</sup>

$$\langle n_{\mathbf{k}} \rangle = \frac{1}{\exp(\hbar\omega_{\mathbf{k}}/k_B T) - 1} . \quad (27)$$

The total number of magnons excited at a temperature  $T$  is

$$\sum_{\mathbf{k}} n_{\mathbf{k}} = \int d\omega D(\omega) \langle n(\omega) \rangle , \quad (28)$$

where  $D(\omega)$  is the number of magnon modes per unit frequency range. The integral is taken over the allowed range of  $\mathbf{k}$ , which is the first Brillouin zone. At sufficiently low temperatures we may evaluate the integral between 0 and  $\infty$  because  $\langle n(\omega) \rangle \rightarrow 0$  exponentially as  $\omega \rightarrow \infty$ .

Magnons have a single polarization for each value of  $\mathbf{k}$ . In three dimensions the number of modes of wavevector less than  $k$  is  $(1/2\pi)^3(4\pi k^3/3)$  per unit volume, whence the number of magnons  $D(\omega)d\omega$  with frequency in  $d\omega$  at  $\omega$  is  $(1/2\pi)^3(4\pi k^2)(dk/d\omega) d\omega$ . In the approximation (25),

$$\frac{d\omega}{dk} = \frac{4JSa^2k}{\hbar} = 2 \left( \frac{2JSa^2}{\hbar} \right)^{1/2} \omega^{1/2} .$$

Thus the density of modes for magnons is

$$D(\omega) = \frac{1}{4\pi^2} \left( \frac{\hbar}{2JSa^2} \right)^{3/2} \omega^{1/2} , \quad (29)$$

so that the total number of magnons is, from (28),

$$\sum_{\mathbf{k}} n_{\mathbf{k}} = \frac{1}{4\pi^2} \left( \frac{\hbar}{2JSa^2} \right)^{3/2} \int_0^\infty d\omega \frac{\omega^{1/2}}{e^{\beta\hbar\omega} - 1} = \frac{1}{4\pi^2} \left( \frac{k_B T}{2JSa^2} \right)^{3/2} \int_0^\infty dx \frac{x^{1/2}}{e^x - 1} .$$

The definite integral is found in tables and has the value  $(0.0587)(4\pi^2)$ .

The number  $N$  of atoms per unit volume is  $Q/a^3$ , where  $Q = 1, 2, 4$  for sc, bcc, fcc lattices, respectively. Now  $(\sum n_{\mathbf{k}})/NS$  is equal to the fractional change of magnetization  $\Delta M/M(0)$ , whence

$$\boxed{\frac{\Delta M}{M(0)} = \frac{0.0587}{SQ} \cdot \left( \frac{k_B T}{2JS} \right)^{3/2}} . \quad (30)$$

<sup>3</sup>The argument is exactly as for phonons or photons. The Planck distribution follows for any problem where the energy levels are identical with those of a harmonic oscillator or collection of harmonic oscillators.

This result is the **Bloch  $T^{3/2}$  law** and has been confirmed experimentally. In neutron scattering experiments spin waves have been observed up to temperatures near the Curie temperature and even above the Curie temperature.

### NEUTRON MAGNETIC SCATTERING

An x-ray photon sees the spatial distribution of electronic charge, whether the charge density is magnetized or unmagnetized. A neutron sees two aspects of a crystal: the distribution of nuclei and the distribution of electronic magnetization. The neutron diffraction pattern for iron is shown in Fig. 11.

The magnetic moment of the neutron interacts with the magnetic moment of the electron. The cross section for the neutron-electron interaction is of the same order of magnitude as for the neutron-nuclear interaction. Diffraction of neutrons by a magnetic crystal allows the determination of the distribution, direction, and order of the magnetic moments.

A neutron can be inelastically scattered by the magnetic structure, with the creation or annihilation of a magnon (Fig. 12); such events make possible the experimental determination of magnon spectra. If the incident neutron has wavevector  $\mathbf{k}_n$  and is scattered to  $\mathbf{k}'_n$  with the creation of a magnon of wavevector  $\mathbf{k}$ , then by conservation of crystal momentum  $\mathbf{k}_n = \mathbf{k}'_n + \mathbf{k} + \mathbf{G}$ , where  $\mathbf{G}$  is a reciprocal lattice vector. By conservation of energy

$$\frac{\hbar^2 k_n'^2}{2M_n} = \frac{\hbar^2 k_n^2}{2M_n} + \hbar\omega_{\mathbf{k}}, \quad (31)$$

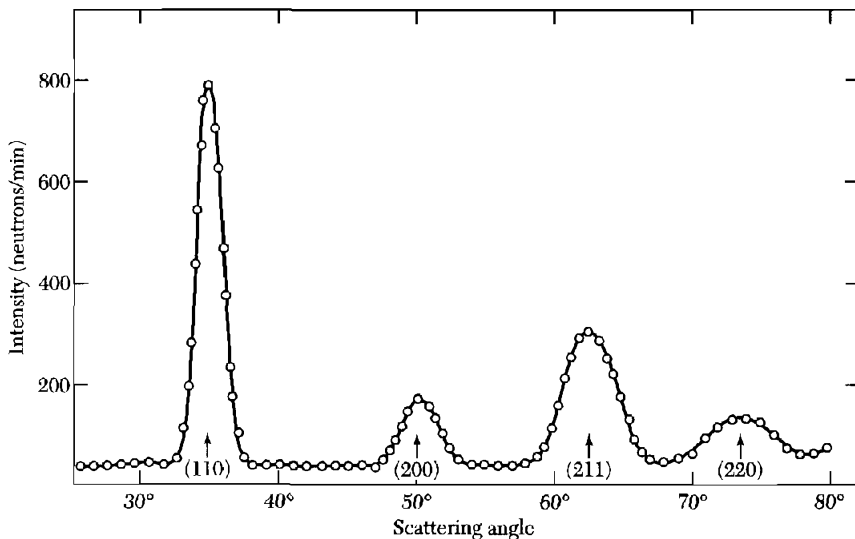


**Figure 11** Neutron diffraction pattern for iron. (After C. G. Shull, E. O. Wollan, and W. C. Koehler.)

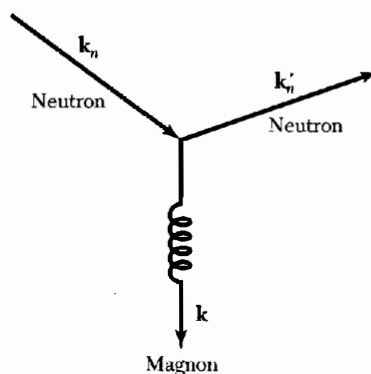


**Figure 12** Scattering of a neutron by an ordered magnetic structure, with creation of a magnon.

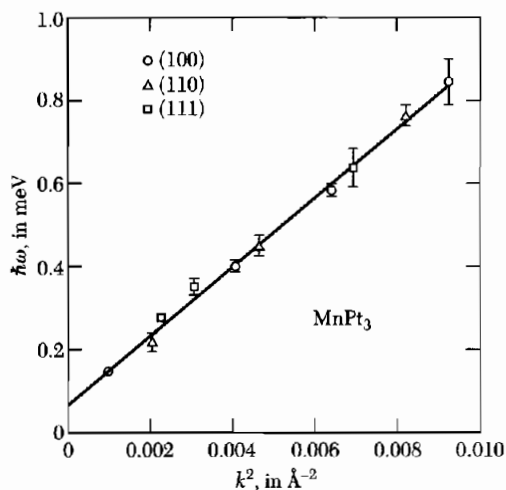


**Figure 13** Magnon energy as a function of the square of the wavevector, for the ferromagnet  $\text{MnPt}_3$ . (After B. Antonini and V. J. Minkiewicz.)

where  $\hbar\omega_k$  is the energy of the magnon created in the process. The observed magnon spectrum for  $\text{MnPt}_3$  is shown in Fig. 13.

### FERRIMAGNETIC ORDER

In many ferromagnetic crystals the saturation magnetization at  $T = 0$  K does not correspond to parallel alignment of the magnetic moments of the constituent paramagnetic ions, even in crystals for which the individual paramagnetic ions have their normal magnetic moments.

The most familiar example is magnetite,  $\text{Fe}_3\text{O}_4$  or  $\text{FeO} \cdot \text{Fe}_2\text{O}_3$ . From Table 11.2 we see that ferric ( $\text{Fe}^{3+}$ ) ions are in a state with spin  $S = \frac{5}{2}$  and

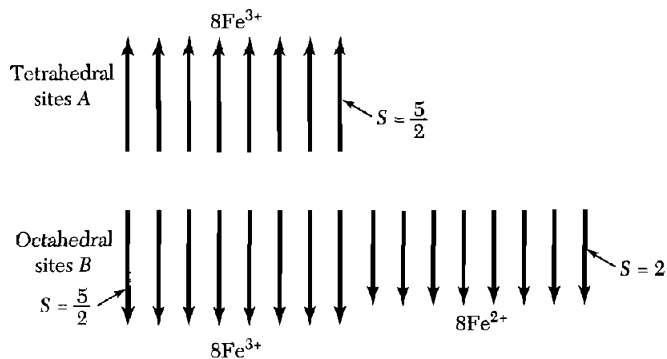


**Figure 14** Spin arrangements in magnetite,  $\text{FeO} \cdot \text{Fe}_2\text{O}_3$ , showing how the moments of the  $\text{Fe}^{3+}$  ions cancel out, leaving only the moments of the  $\text{Fe}^{2+}$  ions.

zero orbital moment. Thus each ion should contribute  $5\mu_B$  to the saturation moment. The ferrous ( $\text{Fe}^{2+}$ ) ions have a spin of 2 and should contribute  $4\mu_B$ , apart from any residual orbital moment contribution. Thus the effective number of Bohr magnetons per  $\text{Fe}_3\text{O}_4$  formula unit should be about  $2 \times 5 + 4 = 14$  if all spins were parallel.

The observed value (Table 1) is 4.1. The discrepancy is accounted for if the moments of the  $\text{Fe}^{3+}$  ions are antiparallel to each other; then the observed moment arises only from the  $\text{Fe}^{2+}$  ion, as in Fig. 14. Neutron diffraction results agree with this model.

A systematic discussion of the consequences of this type of spin order was given by L. Néel with reference to an important class of magnetic oxides known as ferrites. The usual chemical formula of a ferrite is  $\text{MO} \cdot \text{Fe}_2\text{O}_3$ , where M is a divalent cation, often Zn, Cd, Fe, Ni, Cu, Co, or Mg. The term **ferrimagnetic** was coined originally to describe the ferrite-type ferromagnetic spin order such as Fig. 14, and by extension the term covers almost any compound in which some ions have a moment antiparallel to other ions. Many ferrimagnets are poor conductors of electricity, a quality exploited in applications such as rf transformer cores.

The cubic ferrites have the **spinel** crystal structure shown in Fig. 15. There are eight occupied tetrahedral (or A) sites and 16 occupied octahedral (or B) sites in a unit cube. The lattice constant is about 8 Å. A remarkable feature of the spinels is that all exchange integrals  $J_{AA}$ ,  $J_{AB}$ , and  $J_{BB}$  are negative and favor *antiparallel* alignment of the spins connected by the interaction. But the AB interaction is the strongest, so that the A spins are parallel to each other and the B spins are parallel to each other, just in order that the A spins may be antiparallel to the B spins. If  $J$  in  $U = -2J\mathbf{S}_i \cdot \mathbf{S}_j$  is positive, we say that the exchange integral is ferromagnetic; if  $J$  is negative, the exchange integral is antiferromagnetic.

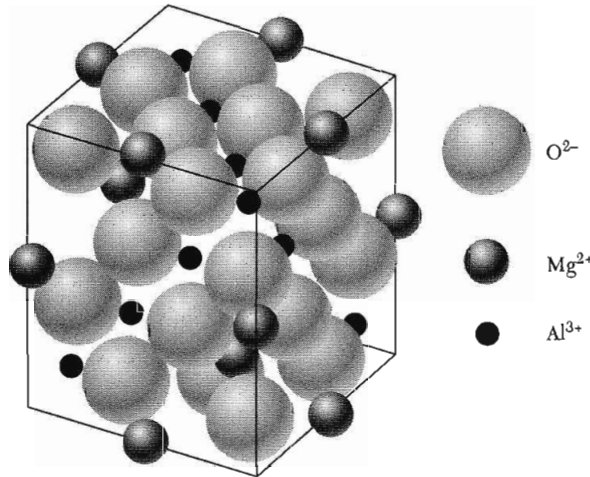


**Figure 15** Crystal structure of the mineral spinel  $\text{MgAl}_2\text{O}_4$ ; the  $\text{Mg}^{2+}$  ions occupy tetrahedral sites, each surrounded by four oxygen ions; the  $\text{Al}^{3+}$  occupy octahedral sites, each surrounded by six oxygen ions. This is a normal spinel arrangement: the divalent metal ions occupy the tetrahedral sites. In the inverse spinel arrangement the tetrahedral sites are occupied by trivalent metal ions, while the octahedral sites are occupied half by divalent and half by trivalent metal ions.

We now prove that three antiferromagnetic interactions can result in ferrimagnetism. The mean exchange fields acting on the  $A$  and  $B$  spin lattices may be written

$$\mathbf{B}_A = -\lambda \mathbf{M}_A - \mu \mathbf{M}_B ; \quad \mathbf{B}_B = -\mu \mathbf{M}_A - \nu \mathbf{M}_B ; \quad (32)$$

taking all mean field constants  $\lambda$ ,  $\mu$ ,  $\nu$  to be positive. The minus sign then corresponds to an antiparallel interaction. The interaction energy density is

$$U = -\frac{1}{2}(\mathbf{B}_A \cdot \mathbf{M}_A + \mathbf{B}_B \cdot \mathbf{M}_B) = \frac{1}{2}\lambda M_A^2 + \mu \mathbf{M}_A \cdot \mathbf{M}_B + \frac{1}{2}\nu M_B^2 ; \quad (33)$$

this is lower when  $\mathbf{M}_A$  is antiparallel to  $\mathbf{M}_B$  than when  $\mathbf{M}_A$  is parallel to  $\mathbf{M}_B$ . The energy when antiparallel should be compared with zero, because a possible solution is  $M_A = M_B = 0$ . Thus when

$$\mu M_A M_B > \frac{1}{2}(\lambda M_A^2 + \nu M_B^2) , \quad (34)$$

the ground state will have  $M_A$  directed oppositely to  $M_B$ . (Under certain conditions there may be noncollinear spin arrays of still lower energy.)

### **Curie Temperature and Susceptibility of Ferrimagnets**

We define separate Curie constants  $C_A$  and  $C_B$  for the ions on the  $A$  and  $B$  sites. For simplicity, let all interactions be zero except for an antiparallel interaction between the  $A$  and  $B$  sites:  $\mathbf{B}_A = -\mu \mathbf{M}_B$ ;  $\mathbf{B}_B = -\mu \mathbf{M}_A$ , where  $\mu$  is positive. The same constant  $\mu$  is involved in both expressions because of the form of (33).

We have in the mean field approximation

$$(CGS) \quad M_A T = C_A(B_a - \mu M_B) ; \quad M_B T = C_B(B_a - \mu M_A) , \quad (35)$$

where  $B_a$  is the applied field. These equations have a nonzero solution for  $M_A$  and  $M_B$  in zero applied field if

$$\begin{vmatrix} T & \mu C_A \\ \mu C_B & T \end{vmatrix} = 0 , \quad (36)$$

so that the ferrimagnetic Curie temperature is given by  $T_c = \mu(C_A C_B)^{1/2}$ .

We solve (35) for  $M_A$  and  $M_B$  to obtain the susceptibility at  $T > T_c$ :

$$(CGS) \quad \chi = \frac{M_A + M_B}{B_a} = \frac{(C_A + C_B)T - 2\mu C_A C_B}{T^2 - T_c^2} , \quad (37)$$

a result more complicated than (4). Experimental values for  $\text{Fe}_3\text{O}_4$  are plotted in Fig. 16. The curvature of the plot of  $1/\chi$  versus  $T$  is a characteristic feature of a ferrimagnet. We consider below the antiferromagnetic limit  $C_A = C_B$ .

**Iron Garnets.** The iron garnets are cubic ferrimagnetic insulators with the general formula  $\text{M}_3\text{Fe}_5\text{O}_{13}$ , where M is a trivalent metal ion and the Fe is the trivalent ferric ion ( $S = \frac{5}{2}$ ,  $L = 0$ ). An example is yttrium iron garnet  $\text{Y}_3\text{Fe}_5\text{O}_{12}$ , known as YIG. Here  $\text{Y}^{3+}$  is diamagnetic.

The net magnetization of YIG is due to the resultant of two oppositely magnetized lattices of  $\text{Fe}^{3+}$  ions. At absolute zero each ferric ion contributes  $\pm 5\mu_B$  to the magnetization, but in each formula unit the three  $\text{Fe}^{3+}$  ions on sites denoted as  $d$  sites are magnetized in one sense and the two  $\text{Fe}^{3+}$  ions on  $a$  sites are magnetized in the opposite sense, giving a resultant of  $5\mu_B$  per formula unit in good agreement with the measurements of Geller *et al.*

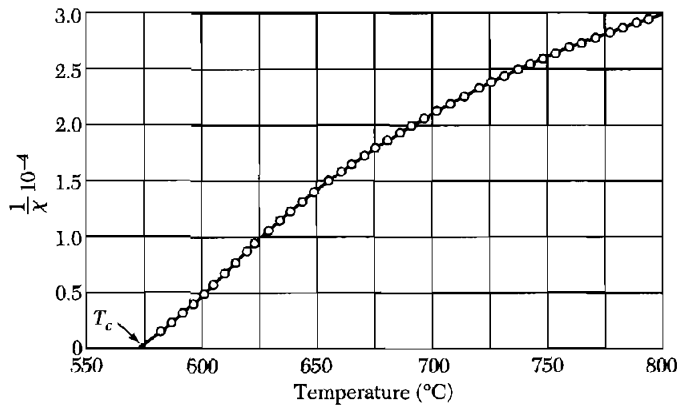


**Figure 16** Reciprocal susceptibility of magnetite,  $\text{FeO} \cdot \text{Fe}_2\text{O}_3$ .

The mean field at an  $a$  site due to the ions on the  $d$  sites is  $B_a = -(1.5 \times 10^4)M_d$ . The observed Curie temperature 559 K of YIG is due to the  $a$ - $d$  interaction. The only magnetic ions in YIG are the ferric ions. Because these are in an  $L = 0$  state with a spherical charge distribution, their interaction with lattice deformations and phonons is weak. As a result YIG is characterized by very narrow linewidths in ferromagnetic resonance experiments.

### ANTIFERROMAGNETIC ORDER

A classical example of magnetic structure determination by neutrons is shown in Fig. 17 for MnO, which has the NaCl structure. At 80 K there are extra neutron reflections not present at 293 K. The reflections at 80 K may be classified in terms of a cubic unit cell of lattice constant 8.85 Å. At 293 K the reflections correspond to an fcc unit cell of lattice constant 4.43 Å.

But the lattice constant determined by x-ray reflection is 4.43 Å at both temperatures, 80 K and 293 K. We conclude that the chemical unit cell has the 4.43 Å lattice parameter, but that at 80 K the electronic magnetic moments of

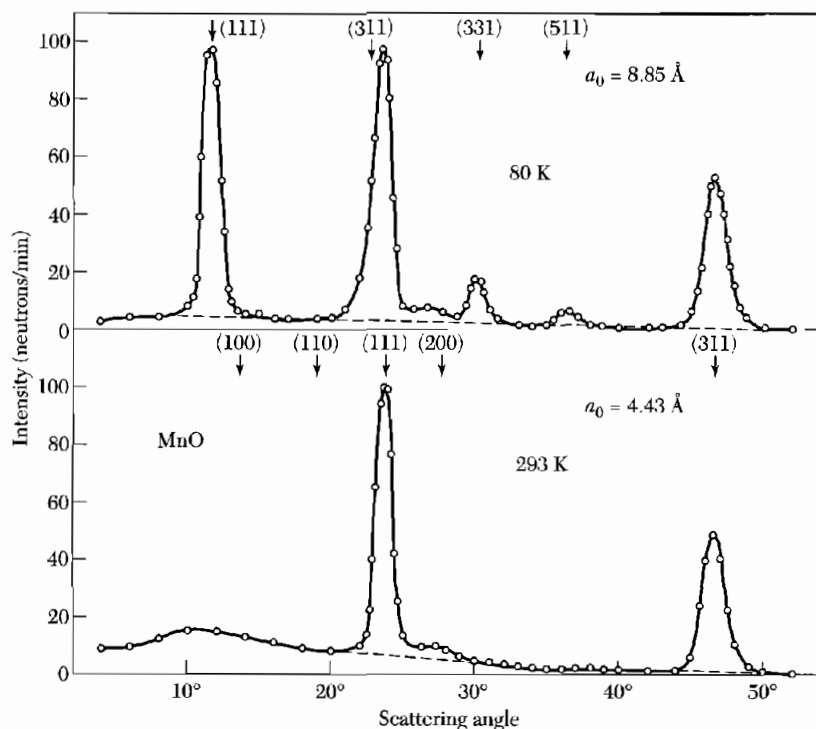


**Figure 17** Neutron diffraction patterns for MnO below and above the spin-ordering temperature of 120 K, after C. C. Shull, W. A. Strauser, and E. O. Wollan. The reflection indices are based on an 8.85 Å cell at 80 K and on a 4.43 Å cell at 293 K. At the higher temperature the  $\text{Mn}^{2+}$  ions are still magnetic, but they are no longer ordered.

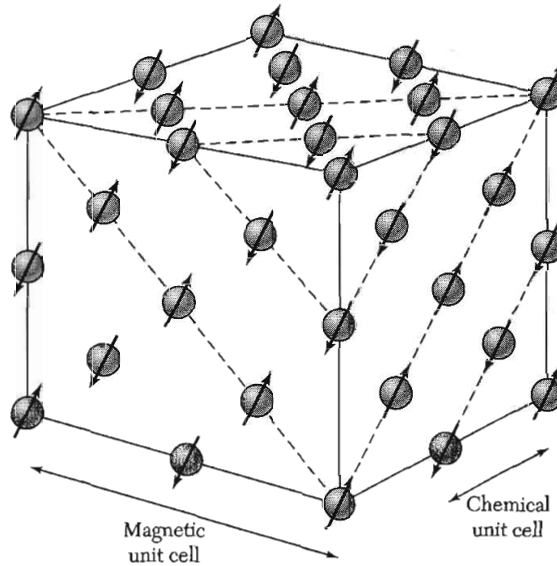


**Figure 18** Ordered arrangements of spins of the  $\text{Mn}^{2+}$  ions in manganese oxide,  $\text{MnO}$ , as determined by neutron diffraction. The  $\text{O}^{2+}$  ions are not shown.

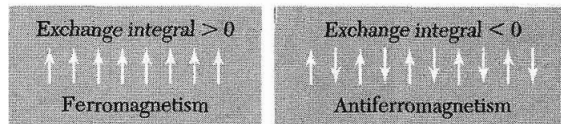


**Figure 19** Spin ordering in ferromagnets ( $J > 0$ ) and antiferromagnets ( $J < 0$ ).

the  $\text{Mn}^{2+}$  ions are ordered in some nonferromagnetic arrangement. If the ordering were ferromagnetic, the chemical and magnetic cells would give the same reflections.

The spin arrangement shown in Fig. 18 is consistent with the neutron diffraction results and with magnetic measurements. The spins in a single [111] plane are parallel, but spins in adjacent [111] planes are antiparallel. Thus  $\text{MnO}$  is an antiferromagnet, as in Fig. 19.

In an **antiferromagnet** the spins are ordered in an antiparallel arrangement with zero net moment at temperatures below the ordering or **Néel temperature** (Table 2). The susceptibility of an antiferromagnet is not infinite at  $T = T_N$ , but has a weak cusp, as in Fig. 20.

An antiferromagnet is a special case of a ferrimagnet for which both sublattices  $A$  and  $B$  have equal saturation magnetizations. Thus  $C_A = C_B$  in (37), and the Néel temperature in the mean field approximation is given by

$$T_N = \mu C \quad , \quad (38)$$

Table 2 Antiferromagnetic crystals

Substance	Paramagnetic ion lattice	Transition temperature, $T_N$ , in K	Curie-Weiss $\theta$ , in K	$\frac{\theta}{T_N}$	$\frac{\chi(0)}{\chi(T_N)}$
MnO	fcc	116	610	5.3	$\frac{2}{3}$
MnS	fcc	160	528	3.3	0.82
MnTe	hex. layer	307	690	2.25	
MnF <sub>2</sub>	bc tetr.	67	82	1.24	0.76
FeF <sub>2</sub>	bc tetr.	79	117	1.48	0.72
FeCl <sub>2</sub>	hex. layer	24	48	2.0	<0.2
FeO	fcc	198	570	2.9	0.8
CoCl <sub>2</sub>	hex. layer	25	38.1	1.53	
CoO	fcc	291	330	1.14	
NiCl <sub>2</sub>	hex. layer	50	68.2	1.37	
NiO	fcc	525	~2000	~4	
Cr	bcc	308			

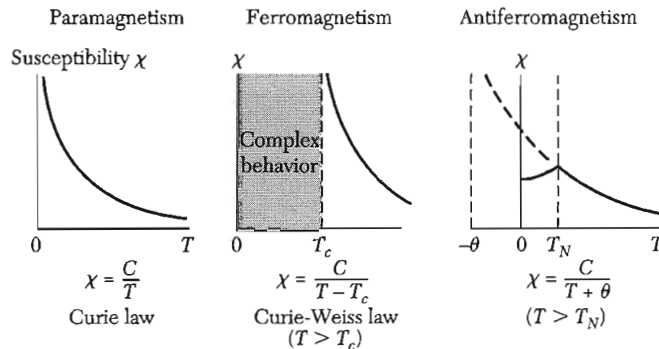


**Figure 20** Temperature dependence of the magnetic susceptibility in paramagnets, ferromagnets, and antiferromagnets. Below the Néel temperature of an antiferromagnet the spins have antiparallel orientations; the susceptibility attains its maximum value at  $T_N$  where there is a well-defined kink in the curve of  $\chi$  versus  $T$ . The transition is also marked by peaks in the heat capacity and the thermal expansion coefficient.

where  $C$  refers to a single sublattice. The susceptibility in the paramagnetic region  $T > T_N$  is obtained from (37):

$$\chi = \frac{2CT - 2\mu C^2}{T^2 - (\mu C)^2} = \frac{2C}{T + \mu C} = \frac{2C}{T + T_N} \quad (39)$$

The experimental results at  $T > T_N$  are of the form

$$(CGS) \quad \chi = \frac{2C}{T + \theta} \quad (40)$$

Experimental values of  $\theta/T_N$  listed in Table 2 often differ substantially from the value unity expected from (39). Values of  $\theta/T_N$  of the observed magnitude may be obtained when next-nearest-neighbor interactions are provided for, and when possible sublattice arrangements are considered. If a mean field constant  $-\epsilon$  is introduced to describe interactions within a sublattice, then  $\theta/T_N = (\mu + \epsilon)/(\mu - \epsilon)$ .

### Susceptibility Below the Néel Temperature

There are two situations: with the applied magnetic field perpendicular to the axis of the spins; and with the field parallel to the axis of the spins. At and above the Néel temperature the susceptibility is nearly independent of the direction of the field relative to the spin axis.

For  $\mathbf{B}_a$  perpendicular to the axis of the spins we can calculate the susceptibility by elementary considerations. The energy density in the presence of the field is, with  $M = |M_A| = |M_B|$ ,

$$U = \mu \mathbf{M}_A \cdot \mathbf{M}_B - \mathbf{B}_a \cdot (\mathbf{M}_A + \mathbf{M}_B) \cong -\mu M^2 [1 - \frac{1}{2}(2\varphi)^2] - 2B_a M \varphi, \quad (41)$$

where  $2\varphi$  is the angle the spins make with each other (Fig. 21a). The energy is a minimum when

$$dU/d\varphi = 0 = 4\mu M^2 \varphi - 2B_a M; \quad \varphi = B_a/2\mu M, \quad (42)$$

so that

$$\text{(CGS)} \quad \chi_{\perp} = 2M\varphi/B_a = 1/\mu. \quad (43)$$

In the parallel orientation (Fig. 21b) the magnetic energy is not changed if the spin systems A and B make equal angles with the field. Thus the susceptibility at  $T = 0$  K is zero:

$$\chi_{\parallel}(0) = 0. \quad (44)$$

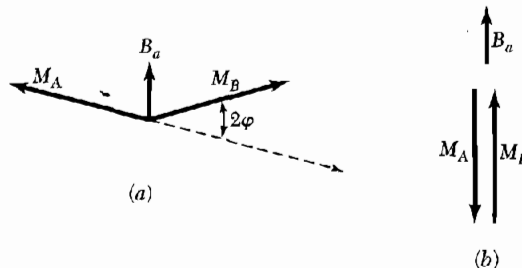


**Figure 21** Calculation of (a) perpendicular and (b) parallel susceptibilities at 0 K, in the mean field approximation.

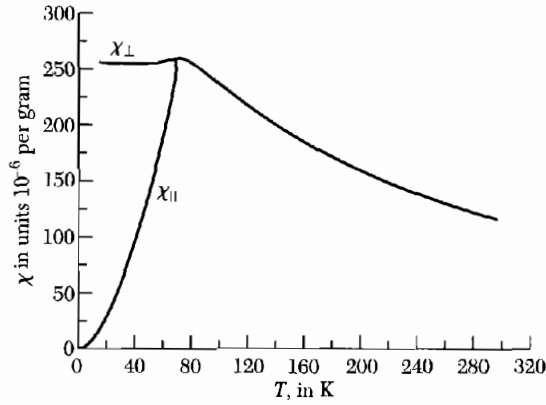


**Figure 22** Magnetic susceptibility of manganese fluoride,  $\text{MnF}_2$ , parallel and perpendicular to the tetragonal axis. (After S. Foner.)

The parallel susceptibility increases smoothly with temperature up to  $T_N$ . Measurements on  $\text{MnF}_2$  are shown in Fig. 22. In very strong fields the spin systems will turn discontinuously from the parallel orientation to the perpendicular orientation where the energy is lower.

### **Antiferromagnetic Magnons**

We obtain the dispersion relation of magnons in a one-dimensional antiferromagnet by making the appropriate substitutions in the treatment (16)–(22) of the ferromagnetic line. Let spins with even indices  $2p$  compose sublattice A, that with spins up ( $S^z = S$ ); and let spins with odd indices  $2p + 1$  compose sublattice B, that with spins down ( $S^z = -S$ ).

We consider only nearest-neighbor interactions, with  $J$  negative. Then (18) written for A becomes, with a careful look at (17),

$$dS_{2p}^x/dt = (2JS/\hbar)(-2S_{2p}^y - S_{2p-1}^y - S_{2p+1}^y) ; \quad (45a)$$

$$dS_{2p}^y/dt = -(2JS/\hbar)(-2S_{2p}^x - S_{2p-1}^x - S_{2p+1}^x) . \quad (45b)$$

The corresponding equations for a spin on B are

$$dS_{2p+1}^x/dt = (2JS/\hbar)(2S_{2p+1}^y + S_{2p}^y + S_{2p+2}^y) ; \quad (46a)$$

$$dS_{2p+1}^y/dt = -(2JS/\hbar)(2S_{2p+1}^x + S_{2p}^x + S_{2p+2}^x) . \quad (46b)$$

We form  $S^+ = S^x + iS^y$ ; then

$$dS_{2p}^+/dt = (2iJS/\hbar)(2S_{2p}^+ + S_{2p-1}^+ + S_{2p+1}^+) ; \quad (47)$$

$$dS_{2p+1}^+/dt = -(2iJS/\hbar)(2S_{2p+1}^+ + S_{2p}^+ + S_{2p+2}^+) . \quad (48)$$

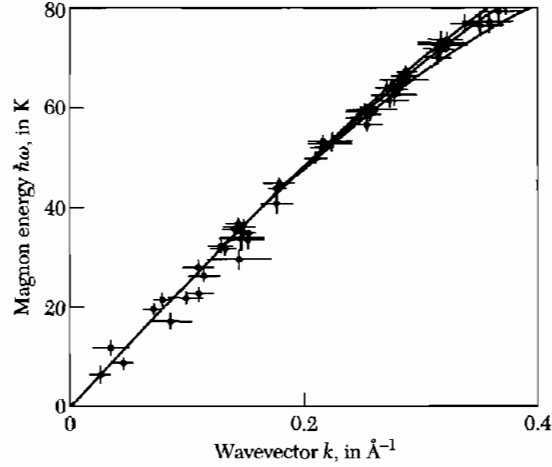


**Figure 23** Magnon dispersion relation in the simple cubic antiferromagnet  $\text{RbMnF}_3$  as determined at 4.2 K by inelastic neutron scattering. (After C. G. Windsor and R. W. H. Stevenson.)

We look for solutions of the form

$$S_{2p}^+ = u \exp[i2pka - i\omega t] ; \quad S_{2p+1}^+ = v \exp[i(2p+1)ka - i\omega t] , \quad (49)$$

so that (47) and (48) become, with  $\omega_{\text{ex}} \equiv -4JS/\hbar = 4|J|S/\hbar$ ,

$$\omega u = \frac{1}{2} \omega_{\text{ex}} (2u + ve^{-ika} + ve^{ika}) ; \quad (50a)$$

$$-\omega v = \frac{1}{2} \omega_{\text{ex}} (2v + ue^{-ika} + ue^{ika}) . \quad (50b)$$

Equations (50) have a solution if

$$\begin{vmatrix} \omega_{\text{ex}} - \omega & \omega_{\text{ex}} \cos ka \\ \omega_{\text{ex}} \cos ka & \omega_{\text{ex}} + \omega \end{vmatrix} = 0 ; \quad (51)$$

$$\text{thus} \quad \omega^2 = \omega_{\text{ex}}^2 (1 - \cos^2 ka) ; \quad \omega = \omega_{\text{ex}} |\sin ka| . \quad (52)$$

The dispersion relation for magnons in an antiferromagnet is quite different from (22) for magnons in a ferromagnet. For  $ka \ll 1$  we see that (52) is linear in  $k$ :  $\omega \cong \omega_{\text{ex}} |ka|$ . The magnon spectrum of  $\text{RbMnF}_3$  is shown in Fig. 23, as determined by inelastic neutron scattering experiments. There is a large region in which the magnon frequency is linear in the wavevector.

Well-resolved magnons have been observed in  $\text{MnF}_2$  at specimen temperatures up to 0.93 of the Néel temperature. Thus even at high temperatures the magnon approximation is useful.

## FERROMAGNETIC DOMAINS

At temperatures well below the Curie point the electronic magnetic moments of a ferromagnet are essentially parallel when regarded on a microscopic scale. Yet, looking at a specimen as a whole, the magnetic moment may be very much less than the saturation moment, and the application of an external magnetic field may be required to saturate the specimen. The behavior observed in polycrystalline specimens is similar to that in single crystals.

Actual specimens are composed of small regions called domains, within each of which the local magnetization is saturated. The directions of magnetization of different domains need not be parallel. An arrangement of domains with approximately zero resultant magnetic moment is shown in Fig. 24. Domains form also in antiferromagnetics, ferroelectrics, antiferroelectrics, ferroelastics, superconductors, and sometimes in metals under conditions of a strong de Haas-van Alphen effect. The increase in the gross magnetic moment of a ferromagnetic specimen in an applied magnetic field takes place by two independent processes:

- In weak applied fields the volume of domains (Fig. 25) favorably oriented with respect to the field increases at the expense of unfavorably oriented domains;

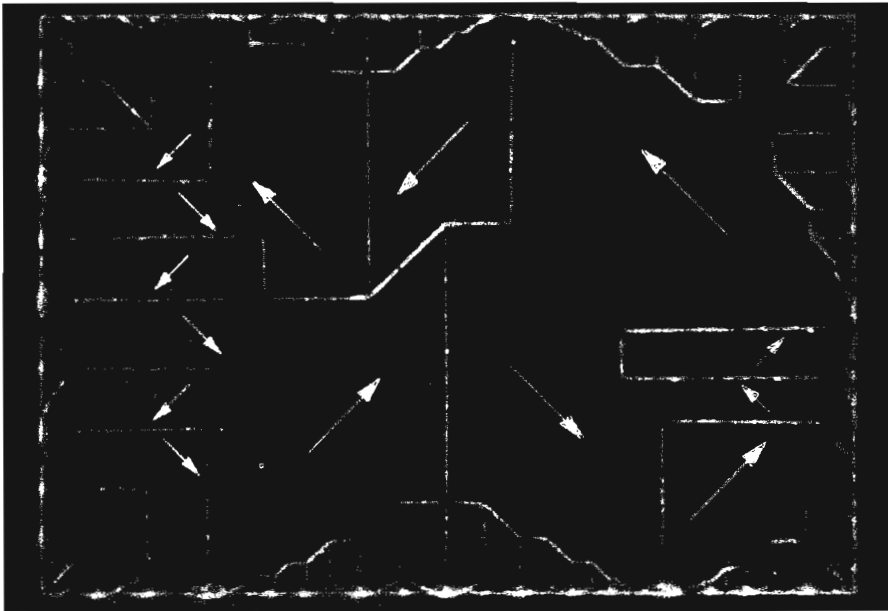


**Figure 24** Ferromagnetic domain pattern on a single crystal platelet of nickel. The domain boundaries are made visible by the Bitter magnetic powder pattern technique. The direction of magnetization within a domain is determined by observing growth or contraction of the domain in a magnetic field. (After R. W. De Blois.)

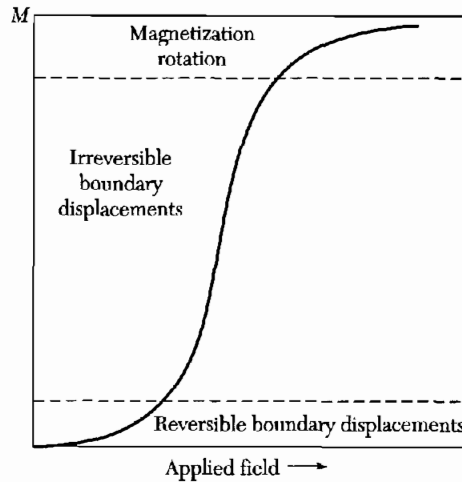


**Figure 25** Representative magnetization curve, showing the dominant magnetization processes in the different regions of the curve.

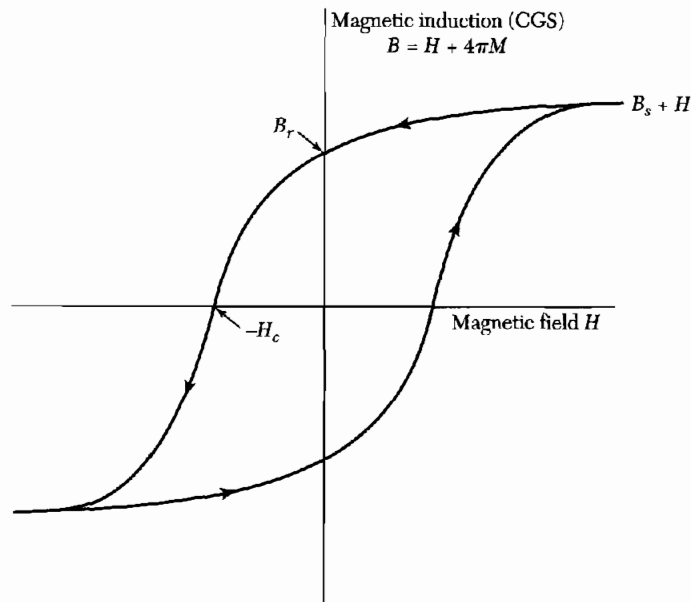


**Figure 26** The technical magnetization curve (or hysteresis loop). The coercivity  $H_c$  is the reverse field that reduces  $B$  to zero; a related coercivity  $H_{ci}$  reduces  $M$  or  $B - H$  to zero. The **remnance**  $B_r$  is the value of  $B$  at  $H = 0$ . The saturation induction  $B_s$  is the limit of  $B - H$  at large  $H$ , and the saturation magnetization  $M_s = B_s/4\pi$ . In SI the vertical axis is  $B = \mu_0(H + M)$ .

- In strong applied fields the domain magnetization rotates toward the direction of the field.

Technical terms defined by the hysteresis loop are shown in Fig. 26. The coercivity is usually defined as the reverse field  $H_c$  that reduces the induction

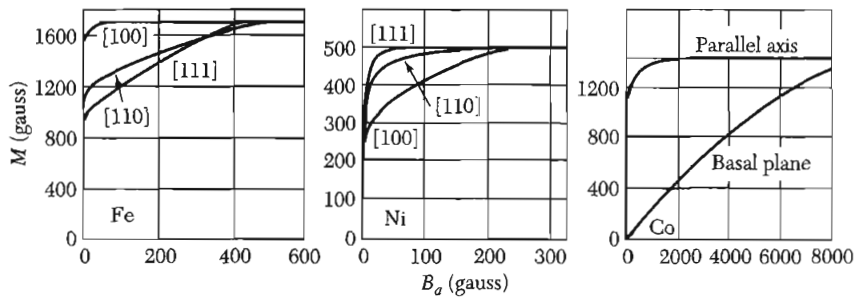


**Figure 27** Magnetization curves for single crystals of iron, nickel, and cobalt. From the curves for iron we see that the [100] directions are easy directions of magnetization and the [111] directions are hard directions. The applied field is  $B_a$ . (After Honda and Kaya.)

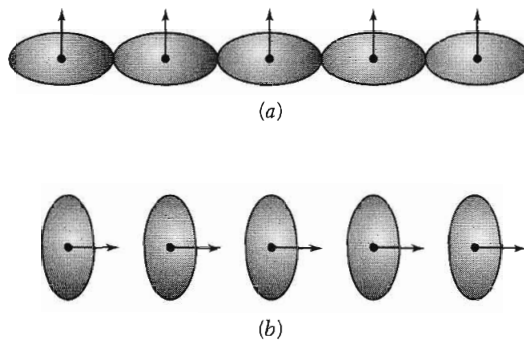


**Figure 28** Asymmetry of the overlap of electron distributions on neighboring ions provides one mechanism of magnetocrystalline anisotropy. Because of spin-orbit interaction the charge distribution is spheroidal and not spherical. The asymmetry is tied to the direction of the spin, so that a rotation of the spin directions relative to the crystal axes changes the exchange energy and also changes the electrostatic interaction energy of the charge distributions on pairs of atoms. Both effects give rise to an anisotropy energy. The energy of (a) is not the same as the energy of (b).

$B$  to zero, starting from saturation. In high coercivity materials the coercivity  $H_{ci}$  is defined as the reverse field that reduces the magnetization  $M$  to zero.

### **Anisotropy Energy**

There is an energy in a ferromagnetic crystal which directs the magnetization along certain crystallographic axes called directions of easy magnetization. This energy is called the **magnetocrystalline** or **anisotropy energy**. It does not come about from the pure isotropic exchange interaction considered thus far.

Cobalt is a hexagonal crystal. The hexagonal axis is the direction of easy magnetization at room temperature, as shown in Fig. 27. One origin of the anisotropy energy is illustrated by Fig. 28. The magnetization of the crystal sees the crystal lattice through orbital overlap of the electrons: the spin interacts

with the orbital motion by means of the spin-orbit coupling. In cobalt the anisotropy energy density is given by

$$U_K = K'_1 \sin^2 \theta + K'_2 \sin^4 \theta , \quad (53)$$

where  $\theta$  is the angle the magnetization makes with the hexagonal axis. At room temperature  $K'_1 = 4.1 \times 10^6$  erg/cm<sup>3</sup>;  $K'_2 = 1.0 \times 10^6$  erg/cm<sup>3</sup>.

Iron is a cubic crystal, and the cube edges are the directions of easy magnetization. To represent the anisotropy energy of iron magnetized in an arbitrary direction with direction cosines  $\alpha_1, \alpha_2, \alpha_3$  referred to the cube edges, we are guided by cubic symmetry. The expression for the anisotropy energy must be an even power of each  $\alpha_i$ , provided opposite ends of a crystal axis are equivalent magnetically, and it must be invariant under interchanges of the  $\alpha_i$  among themselves. The lowest order combination satisfying the symmetry requirements is  $\alpha_1^2 + \alpha_2^2 + \alpha_3^2$ , but this is identically equal to unity and does not describe anisotropy effects. The next combination is of the fourth degree:  $\alpha_1^2 \alpha_2^2 + \alpha_1^2 \alpha_3^2 + \alpha_3^2 \alpha_2^2$ , and then of the sixth degree:  $\alpha_1^2 \alpha_2^2 \alpha_3^2$ . Thus

$$U_K = K_1(\alpha_1^2 \alpha_2^2 + \alpha_2^2 \alpha_3^2 + \alpha_3^2 \alpha_1^2) + K_2 \alpha_1^2 \alpha_2^2 \alpha_3^2 . \quad (54)$$

At room temperature in iron  $K_1 = 4.2 \times 10^5$  erg/cm<sup>3</sup> and  $K_2 = 1.5 \times 10^5$  erg/cm<sup>3</sup>.

### Transition Region Between Domains

A **Bloch wall** in a crystal is the transition layer that separates adjacent regions (domains) magnetized in different directions. The entire change in spin direction between domains does not occur in one discontinuous jump across a single atomic plane, but takes place in a gradual way over many atomic planes (Fig. 29). The exchange energy is lower when the change is distributed over many spins. This behavior may be understood by interpreting the Heisenberg equation (6) classically. We replace  $\cos \varphi$  by  $1 - \frac{1}{2}\varphi^2$ ; then  $w_{\text{ex}} = JS^2\varphi^2$  is the exchange energy between two spins making a small angle  $\varphi$  with each other. Here  $J$  is the exchange integral and  $S$  is the spin quantum number;  $w_{\text{ex}}$  is referred to the energy for parallel spins.

If a total change of  $\pi$  occurs in  $N$  equal steps, the angle between neighboring spins is  $\pi/N$ , and the exchange energy per pair of neighboring atoms is  $w_{\text{ex}} = JS^2(\pi/N)^2$ . The total exchange energy of a line of  $N + 1$  atoms is

$$Nw_{\text{ex}} = JS^2\pi^2/N . \quad (55)$$

The wall would thicken without limit were it not for the anisotropy energy, which acts to limit the width of the transition layer. The spins contained within the wall are largely directed away from the axes of easy magnetization, so there is an anisotropy energy associated with the wall, roughly proportional to the wall thickness.

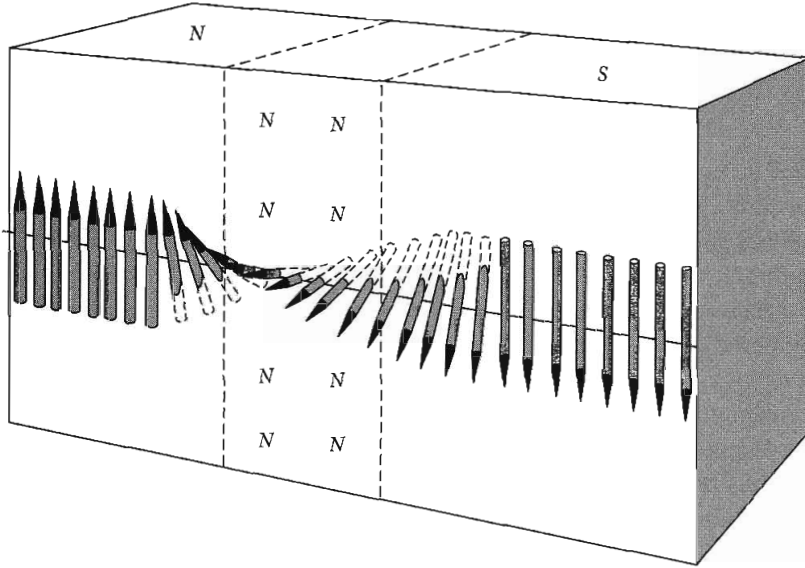


**Figure 29** The structure of the Bloch wall separating domains. In iron the thickness of the transition region is about 300 lattice constants.

Consider a wall parallel to the cube face of a simple cubic lattice and separating domains magnetized in opposite directions. We wish to determine the number  $N$  of atomic planes contained within the wall. The energy per unit area of wall is the sum of contributions from exchange and anisotropy energies:  $\sigma_w = \sigma_{ex} + \sigma_{anis}$ .

The exchange energy is given approximately by (55) for each line of atoms normal to the plane of the wall. There are  $1/a^2$  such lines per unit area, where  $a$  is the lattice constant. Thus  $\sigma_{ex} = \pi^2 JS^2 / Na^2$  per unit area of wall.

The anisotropy energy is of the order of the anisotropy constant times the thickness  $Na$ , or  $\sigma_{anis} \approx KNa$ ; therefore

$$\sigma_w \approx (\pi^2 JS^2 / Na^2) + KNa . \quad (56)$$

This is a minimum with respect to  $N$  when

$$\partial \sigma_w / \partial N = 0 = -(\pi^2 JS^2 / N^2 a^2) + Ka ; \quad (57)$$

or

$$N = (\pi^2 JS^2 / Ka^3)^{1/2} . \quad (58)$$

For order of magnitude,  $N \approx 300$  in iron.

The total wall energy per unit area on our model is

$$\sigma_w = 2\pi(KJS^2/a)^{1/2} ; \quad (59)$$

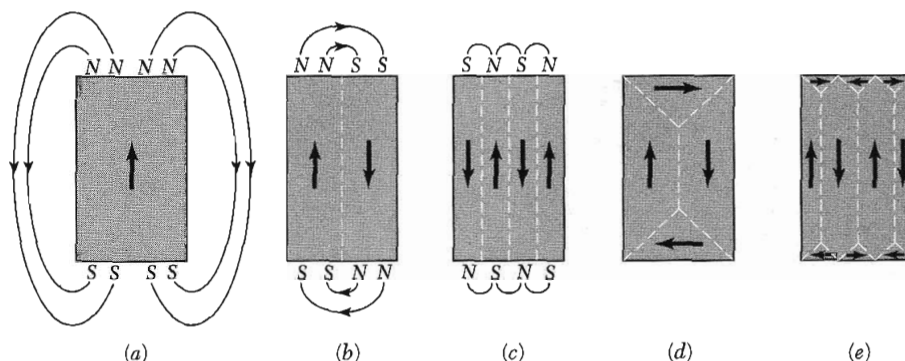


Figure 30 The origin of domains.

in iron  $\sigma_w \approx 1 \text{ erg/cm}^2$ . Accurate calculation for a  $180^\circ$  wall in a (100) plane gives  $\sigma_w = 2(2K_1JS^2/a)^{1/2}$ .

### Origin of Domains

Landau and Lifshitz showed that domain structure is a natural consequence of the various contributions to the energy—exchange, anisotropy, and magnetic—of a ferromagnetic body.

Direct evidence of domain structure is furnished by photomicrographs of domain boundaries obtained by the technique of magnetic powder patterns and by optical studies using Faraday rotation. The powder pattern method developed by F. Bitter consists in placing a drop of a colloidal suspension of finely divided ferromagnetic material, such as magnetite, on the surface of the ferromagnetic crystal. The colloid particles in the suspension concentrate strongly about the boundaries between domains where strong local magnetic fields exist which attract the magnetic particles. The discovery of transparent ferromagnetic compounds has encouraged the use also of optical rotation for domain studies.

We may understand the origin of domains by considering the structures shown in Fig. 30, each representing a cross section through a ferromagnetic single crystal. In (a) we have a single domain; as a consequence of the magnetic "poles" formed on the surfaces of the crystal this configuration will have a high value of the magnetic energy  $(1/8\pi) \int B^2 dV$ . The magnetic energy density for the configuration shown will be of the order of  $M_s^2 \approx 10^6 \text{ erg/cm}^3$ ; here  $M_s$  denotes the saturation magnetization, and the units are CGS.

In (b) the magnetic energy is reduced by roughly one-half by dividing the crystal into two domains magnetized in opposite directions. In (c) with  $N$  domains the magnetic energy is reduced to approximately  $1/N$  of the magnetic energy of (a), because of the reduced spatial extension of the field.



**Figure 31** Domain of closure at the end of a single crystal iron whisker. The face is a (100) plane; the whisker axis is [001]. (Courtesy of R. V. Coleman, C. G. Scott, and A. Isin.)

In domain arrangements such as (d) and (e) the magnetic energy is zero. Here the boundaries of the triangular prism domains near the end faces of the crystal make equal angles ( $45^\circ$ ) with the magnetization in the rectangular domains and with the magnetization in the domains of closure. The component of magnetization normal to the boundary is continuous across the boundary and there is no magnetic field associated with the magnetization. The flux circuit is completed within the crystal—thus giving rise to the term **domains of closure** for surface domains that complete the flux circuit, as in Fig. 31.

Domain structures are often more complicated than our simple examples, but *domain structure always has its origin in the possibility of lowering the energy of a system by going from a saturated configuration with high magnetic energy to a domain configuration with a lower energy.*

### **Coercivity and Hysteresis**

The coercivity is the magnetic field  $H_c$  required to reduce the magnetization or the induction  $B$  to zero (Fig. 26). The value of the coercivity ranges over seven orders of magnitude; it is the most sensitive property of ferromagnetic materials which is subject to control. The coercivity may vary from 600 G in a loudspeaker permanent magnet (Alnico V) and 10,000 G in a special high stability magnet ( $\text{SmCo}_5$ ) to 0.5 G in a commercial power transformer (Fe-Si 4 wt. pct.) and 0.002 G in a pulse transformer (Supermalloy). Low coercivity is desired in a transformer, for this means low hysteresis loss per cycle of operation. Materials with low coercivity are called **soft**; those with high coercivity are called **hard**, although there is not necessarily a 1 : 1 relationship of magnetic hardness with mechanical hardness.

The coercivity decreases as the impurity content decreases and also as internal strains are removed by annealing (slow cooling). Amorphous ferromagnetic alloys may have low coercivity, low hysteresis losses, and high permeability. Alloys that contain a precipitated phase may have a high coercivity, as in Alnico V (Fig. 32).

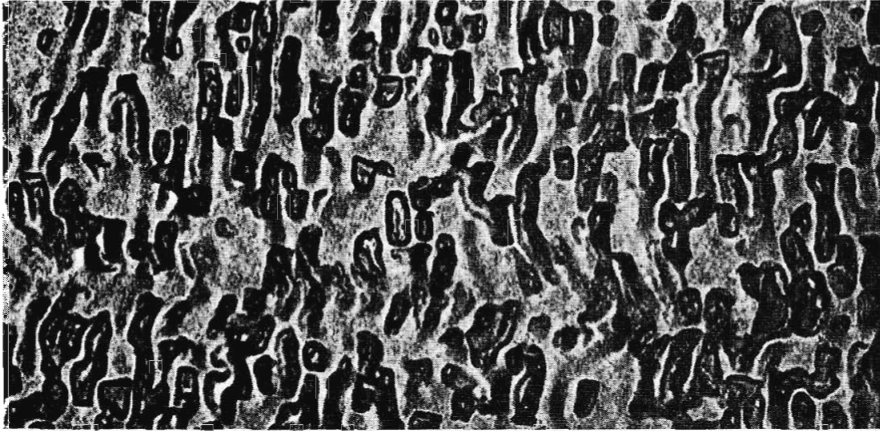


**Figure 32** Microstructure of Alnico V in its optimum state as a permanent magnet. The composition of Alnico V is, by weight percent, 8 Al, 14 Ni, 24 Co, 3 Cu, 51 Fe. As a permanent magnet it is a two-phase system, with fine particles of one phase embedded in the other phase. The precipitation is carried out in a magnetic field, and the particles are oriented with their long axis parallel to the field direction. The width shown is  $1.1 \mu\text{m}$ . (Courtesy of F. E. Luborsky.)

Soft magnetic materials are used to concentrate and shape magnetic flux, as in motors, generators, transformers, and sensors. Useful soft materials include electrical steels (usually alloyed with several percent of silicon to increase electrical resistivity and to decrease anisotropy); various alloys of Fe-Co-Mn, starting with permalloys of composition near  $\text{Ni}_{78}\text{Fe}_{22}$ , which have near-zero anisotropy energy and near-zero magnetostriction; NiZn and MnZn ferrites; and metallic glasses produced by rapid solidification. A commercial metallic glass (METGLAS 2605S-2) with composition  $\text{Fe}_{79}\text{B}_{13}\text{Si}_9$  has a hysteresis loss per cycle much lower than the best grain-oriented silicon steel.

The high coercivity of materials composed of very small grains or fine powders is well understood. A sufficiently small particle, with diameter less than  $10^{-5}$  or  $10^{-6}$  cm, is always magnetized to saturation as a single domain because the formation of a flux-closure configuration is energetically unfavorable. In a single domain particle it is not possible for magnetization reversal to take place by means of the process of boundary displacement, which usually requires relatively weak fields. Instead the magnetization of the particle must rotate as a whole, a process that may require large fields depending on the anisotropy energy of the material and the anisotropy of the shape of the particle.

The coercivity of fine iron particles is expected theoretically to be about 500 gauss on the basis of rotation opposed by the crystalline anisotropy energy, and this is of the order of the observed value. Higher coercivities have been

reported for elongated iron particles, the rotation here being opposed by the shape anisotropy of the demagnetization energy.

Rare earth metals in alloys with Mn, Fe, Co, and Ni have very large crystal anisotropies  $K$  and correspondingly large coercivities, of the order of  $2K/M$ . These alloys are exceptionally good permanent magnets. For example, the hexagonal compound  $\text{SmCo}_5$  has an anisotropy energy  $1.1 \times 10^8 \text{ erg cm}^{-3}$ , equivalent to a coercivity  $2K/M$  of 290 kG (29 T). Magnets of  $\text{Nd}_2\text{Fe}_{14}\text{B}$  have energy products as high as 50 MGOe, exceeding all other commercially available magnets.

### SINGLE-DOMAIN PARTICLES

The dominant industrial and commercial applications of ferromagnetism are in magnetic recording devices, where the magnetic material is in the form of single-domain particles or regions. The total value of the production of magnetic devices for recording may be comparable with the total value of semiconductor device production and greatly exceeds the value of superconducting device production, the latter being held back by low critical temperatures, as compared with magnetic Curie temperatures. The magnetic recording devices or memories typically are in the form of hard disks in computers and tape in video and audio recorders.

An ideal single-domain particle is a fine particle, usually elongated, that has its magnetic moment directed toward one end or the other of the particle. The alternative orientations may be labeled as N or S; + or -; in digital recording, as 0 or 1. To have digital properties a ferromagnetic particle should be fine enough, typically 10–100 nm, so that only one domain is within the particle. If the fine particle is elongated (acicular) or has uniaxial crystal symmetry, only two values of the magnetic moment of the single domain are permitted, which is what one wants for digital properties. The first successful recording material was acicular  $\gamma\text{-Fe}_2\text{O}_3$  with length-to-width ratio of about 5 : 1, coercivity near 200 Oe and a length  $< 1 \mu\text{m}$ ; chromium dioxide  $\text{CrO}_2$  is the basis of a better material, in a form highly acicular (20 : 1) with coercivity near 500 Oe.

Effective elongation can be attained with spheres by making a chain, like a string of beads. An ensemble of such chains or of elongated single domain particles is said to exhibit **superparamagnetism** if the magnetic moment of a unit is constant. If  $\mu$  is the magnetic moment in a magnetic field  $B$ , then the net magnetization of the ensemble will follow the Curie-Brillouin-Langevin law of Chapter 11 if the particles are embedded in a liquid so that they are each free to rotate as a whole. If the particles are frozen in a solid, there will be a remanent magnetization (Fig. 26) after removal of an applied field.

### ***Geomagnetism and Biomagnetism***

Single domain ferromagnetic properties are of special geological interest in sedimentary rocks because the rocks through their remanent magnetization carry a memory of the direction of the earth's magnetic field at the time that they were laid down, and thus of the geographical location of the rocks at that epoch. The magnetic record is perhaps the most important basis of the theory of the drift of continents. Annually, layers of sediment are deposited in stream beds, layers that may bear some magnetic particles in single domain form. This record persists over at least 500 million years of geological time and can tell us where on the surface of the earth the deposit was laid down at a given time. Lava flows also record magnetic field directions.

The change in magnetization from layer to layer gives a superb historical record of the drift of the continental plates on the earth's surface. The paleomagnetic record is one basis of the branch of geology called plate tectonics. The original interpretation of the record was made more difficult, or more exciting, by the associated discovery (Brunhes, 1906) that the magnetic field of the earth itself can show reversals in direction, an effect contained within the standard dynamo theory of the earth's magnetism. Reversals have taken place once every  $1 \times 10^4$  to  $25 \times 10^6$  years. When a reversal occurs, it is relatively sudden.

Fine single domain particles, often of magnetite  $\text{Fe}_3\text{O}_4$ , are even of importance in biology. A direction-seeking effect known as **magnetotaxis** often controls, possibly sometimes along with an astronomical guide system, the motion of bacteria, the migration of birds, and the movements of homing pigeons and bees. The effect is due to the interaction of a single domain particle (or cluster of such particles, Fig. 33) in the organism with the external magnetic field of the earth.

### ***Magnetic Force Microscopy***

The success of the scanning tunneling microscope (STM) stimulated the development of related scanning probe devices, of which the scanning magnetic force microscope is one of the most effective. A sharp tip of a magnetic material, such as nickel, is mounted on a cantilever lever (Fig. 34). Ideally, but not yet, the tip is a single domain particle. Forces from the magnetic sample act on the tip and cause a change, such as a deflection, in the cantilever status, and an image is formed by scanning the sample relative to the tip. The magnetic force microscope (MFM) is the only magnetic imaging technique that can provide high resolution (10–100 nm) with little surface preparation. One can, for example, observe and image the magnetic flux that exits from the surface at the intersection of a Bloch wall with the surface (Fig. 29). An important application is to the study of magnetic recording media—Figure 35 shows the magnetic signal from a test pattern of  $2 \mu\text{m}$  bits magnetized in the plane of

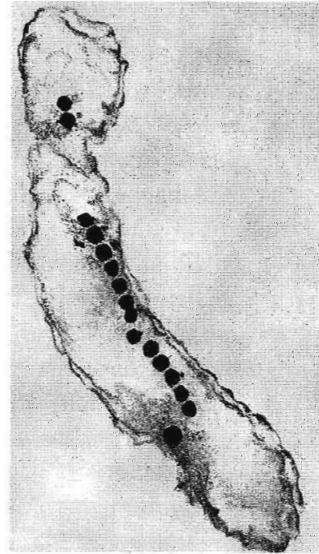


**Figure 33** Thin section of a cell of a magnetotactic bacterium showing a chain of 50 nm particles of  $\text{Fe}_3\text{O}_4$ . Drawing by Marta Puebla from a photograph by R. B. Frankel and others.

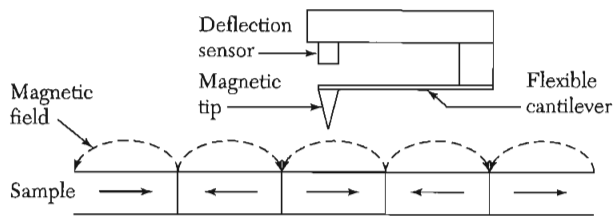


**Figure 34** Basic concept of magnetic force microscopy. A magnetic tip attached to a flexible cantilever is used to detect the magnetic field produced by the regions of alternating magnetization in the plane of the sample. (After Gruetter, Mamin, and Rugar, 1992.)

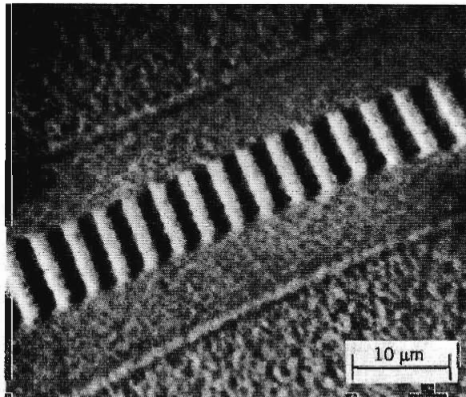


**Figure 35** Test strip magnetization in the plane of a Co-alloy disk in  $2\ \mu\text{m}$  bits, as detected by MFM close above the plane of the disk. (After Rugar et al.)

a Co-alloy disk; the parallel component of the field seen by the sensor tip is what the photo shows.

### SUMMARY

(In CGS Units)

- The susceptibility of a ferromagnet above the Curie temperature has the form  $\chi = C/(T - T_c)$  in the mean field approximation.
- In the mean field approximation the effective magnetic field seen by a magnetic moment in a ferromagnet is  $\mathbf{B}_a + \lambda\mathbf{M}$ , when  $\lambda = T_c/C$  and  $\mathbf{B}_a$  is the applied magnetic field.
- The elementary excitations in a ferromagnet are magnons. Their dispersion relation for  $ka \ll 1$  has the form  $\hbar\omega \approx Jk^2a^2$  in zero external magnetic field. The thermal excitation of magnons leads at low temperatures to a heat capacity and to a fractional magnetization change both proportional to  $T^{3/2}$ .
- In an antiferromagnet two spin lattices are equal, but antiparallel. In a ferrimagnet two lattices are antiparallel, but the magnetic moment of one is larger than the magnetic moment of the other.
- In an antiferromagnet the susceptibility above the Néel temperature has the form  $\chi = 2C/(T + \theta)$ .
- The magnon dispersion relation in an antiferromagnet has the form  $\hbar\omega \approx Jka$ . The thermal excitation of magnons leads at low temperatures to a term in  $T^3$  in the heat capacity, in addition to the phonon term in  $T^3$ .
- A Bloch wall separates domains magnetized in different directions. The thickness of a wall is  $\approx (J/Ka^3)^{1/2}$  lattice constants, and the energy per unit area is  $\approx (KJ/a)^{1/2}$ , where  $K$  is the anisotropy energy density.

### Problems

1. **Magnon dispersion relation.** Derive the magnon dispersion relation (24) for a spin  $S$  on a simple cubic lattice,  $z = 6$ . Hint: Show first that (18a) is replaced by

$$dS_{\rho}^x/dt = (2JS/\hbar)(6S_{\rho}^y - \sum_{\delta} S_{\rho+\delta}^y),$$

where the central atom is at  $\rho$  and the six nearest neighbors are connected to it by six vectors  $\delta$ . Look for solutions of the equations for  $dS_{\rho}^x/dt$  and  $dS_{\rho}^y/dt$  of the form  $\exp(i\mathbf{k} \cdot \rho - i\omega t)$ .

2. **Heat capacity of magnons.** Use the approximate magnon dispersion relation  $\omega = Ak^2$  to find the leading term in the heat capacity of a three-dimensional ferromagnet at low temperatures  $k_B T \ll J$ . The result is  $0.113 k_B (k_B T/\hbar A)^{3/2}$ , per unit

volume. The zeta function that enters the result may be estimated numerically; it is tabulated in Jahnke-Emde.

3. **Néel temperature.** Taking the effective fields on the two-sublattice model of an antiferromagnetic as

$$B_A = B_a - \mu M_B - \epsilon M_A ; \quad B_B = B_a - \mu M_A - \epsilon M_B ,$$

show that

$$\frac{\theta}{T_N} = \frac{\mu + \epsilon}{\mu - \epsilon} .$$

4. **Magnetoelastic coupling.** In a cubic crystal the elastic energy density in terms of the usual strain components  $e_{ij}$  is (Chapter 3)

$$U_d = \frac{1}{2}C_{11}(e_{xx}^2 + e_{yy}^2 + e_{zz}^2) + \frac{1}{2}C_{44}(e_{xy}^2 + e_{yz}^2 + e_{zx}^2) + C_{12}(e_{yy}e_{zz} + e_{xx}e_{zz} + e_{xx}e_{yy}) ,$$

and the leading term in the magnetic anisotropy energy density is, from (54),

$$U_K = K_1(\alpha_1^2\alpha_2^2 + \alpha_2^2\alpha_3^2 + \alpha_3^2\alpha_1^2) .$$

Coupling between elastic strain and magnetization direction may be taken formally into account by including in the total energy density a term

$$U_c = B_1(\alpha_1^2e_{xx} + \alpha_2^2e_{yy} + \alpha_3^2e_{zz}) + B_2(\alpha_1\alpha_2e_{xy} + \alpha_2\alpha_3e_{yz} + \alpha_3\alpha_1e_{zx})$$

arising from the strain dependence of  $U_K$ ; here  $B_1$  and  $B_2$  are called magnetoelastic coupling constants. Show that the total energy is a minimum when

$$e_{ii} = \frac{B_1[C_{12} - \alpha_i^2(C_{11} + 2C_{12})]}{[(C_{11} - C_{12})(C_{11} + 2C_{12})]} ; \quad e_{ij} = -\frac{B_2\alpha_i\alpha_j}{C_{44}} \quad (i \neq j) .$$

This explains the origin of magnetostriction, the change of length on magnetization.

5. **Coercive force of a small particle.** (a) Consider a small spherical single-domain particle of a uniaxial ferromagnet. Show that the reverse field along the axis required to reverse the magnetization is  $B_a = 2K/M_s$ , in CGS units. The coercive force of single-domain particles is observed to be of this magnitude. Take  $U_K = K \sin^2 \theta$  as the anisotropy energy density and  $U_M = -B_a M \cos \theta$  as the interaction energy density with the external field; here  $\theta$  is the angle between  $\mathbf{B}_a$  and  $\mathbf{M}$ . Hint: Expand the energies for small angles about  $\theta = \pi$ , and find the value of  $B_a$  for which  $U_K + U_M$  does not have a minimum near  $\theta = \pi$ . (b) Show that the magnetic energy of a saturated sphere of diameter  $d$  is  $\approx M_s^2 d^3$ . An arrangement with appreciably less magnetic energy has a single wall in an equatorial plane. The domain wall energy will be  $\pi\sigma_w d^2/4$ , where  $\sigma_w$  is the wall energy per unit area. Estimate for cobalt the critical radius below which the particles are stable as single domains, taking the value of  $JS^2/a$  as for iron.
6. **Saturation magnetization near  $T_c$ .** Show that in the mean field approximation the saturation magnetization just below the Curie temperature has the dominant

temperature dependence  $(T_c - T)^{1/2}$ . Assume the spin is  $\frac{1}{2}$ . The result is the same as that for a second-order transition in a ferroelectric crystal, as discussed in Chapter 16. The experimental data for ferromagnets (Table 1) suggest that the exponent is closer to 0.33.

7. **Néel wall.** The direction of magnetization change in a domain wall goes from that of the Bloch wall to that of a Néel wall (Fig. 36) in thin films of material of negligible crystalline anisotropy energy, such as Permalloy. The intercept of the Bloch wall with the surface of the film creates a surface region of high demagnetization energy. The Néel wall avoids this intercept contribution, but at the expense of a demagnetization contribution throughout the volume of the wall. The Néel wall becomes energetically favorable when the film becomes sufficiently thin. Consider, however, the energetics of the Néel wall in bulk material of negligible crystalline anisotropy energy. There is now a demagnetization contribution to the wall energy density. By a qualitative argument similar to (56), show that  $\sigma_w \approx (\pi^2 JS^2/Na^2) + (2\pi M_s^2 Na)$ . Find  $N$  for which  $\sigma_w$  is a minimum. Estimate the order of magnitude of  $\sigma_w$  for typical values of  $J$ ,  $M_s$ , and  $a$ .
8. **Giant magnetoresistance.** In a ferromagnetic metal, the conductivity  $\sigma_p$  for electrons whose magnetic moments are oriented parallel to the magnetization is typically larger than  $\sigma_a$  for those antiparallel to the magnetization. Consider a ferromagnetic conductor consisting of two separate regions of identical dimensions in series whose magnetizations can be independently controlled. Electrons of a given spin flow first through one region and then through the other. It is observed that the resistance when both magnetizations point upwards,  $R_{\uparrow\uparrow}$ , is lower than the resistance when they point opposite,  $R_{\uparrow\downarrow}$ . This resistance change can be large for  $\sigma_p/\sigma_a \gg 1$ , and the phenomenon is called giant magnetoresistance (GMR). A small external magnetic field can switch the resistance from  $R_{\uparrow\downarrow}$  to  $R_{\uparrow\uparrow}$  by reorienting the magnetization of the second layer. This effect is increasingly used in magnetic storage applications such as the magnetic bit readout in hard drives. The giant magnetoresistance ratio is defined as:

$$GMRR = \frac{R_{\uparrow\downarrow} - R_{\uparrow\uparrow}}{R_{\uparrow\uparrow}}.$$

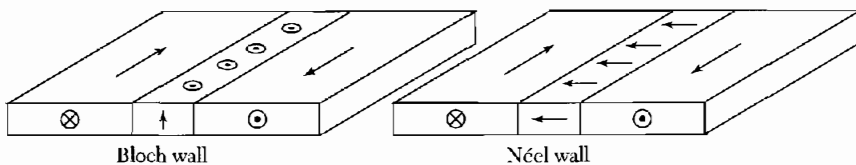


**Figure 36** A Bloch wall and a Néel wall in a thin film. The magnetization in the Bloch wall is normal to the plane of the film and adds to the wall energy a demagnetization energy  $\sim M_s^2 \delta d$  per unit length of wall, where  $\delta$  is the wall thickness and  $d$  the film thickness. In the Néel wall the magnetization is parallel to the surface: the addition to the wall energy is negligible when  $d \ll \delta$ . The addition to the Néel wall energy when  $d \gg \delta$  is the subject of Problem 7. (After S. Middelhock.)

(a) If there is no spin-flip scattering for the conduction electrons, show that

$$GMRR = (\sigma_p/\sigma_a + \sigma_a/\sigma_p - 2)/4$$

(Hint: Treat the spin-up and spin-down conduction electrons as independent conducting channels in parallel.) (b) If  $\sigma_a \rightarrow 0$ , explain physically why the resistance in the  $\uparrow\downarrow$  magnetization configuration is infinite.